

CLASSICAL AND QUANTUM MANY-BODY
DESCRIPTION
OF BREMSSTRAHLUNG IN DENSE MATTER
(Landau - Pomeranchuk - Migdal Effect)

Jörn Knoll and Dmitri N. Voskresensky ¹

*Gesellschaft für Schwerionenforschung GSI
P.O.Box 110552, D-64220 Darmstadt, Germany*

Abstract

Some considerations about the importance of coherence effects for bremsstrahlung processes in non-equilibrium dense matter (Landau - Pomeranchuk - Migdal - effect) are presented. They are of particular relevance for the application to photon - and di-lepton production from high energy nuclear collisions, to gluon radiation in QCD transport, or parton kinetics and to neutrino and axion radiation from supernova explosion and from hot neutron stars. The soft behavior of the bremsstrahlung from a source described by classical transport models is discussed and pocket correction formulas for the in-matter radiation cross sections are suggested in terms of standard transport coefficients. The radiation rates are also discussed within a non-equilibrium quantum field theory (Schwinger - Kadanoff - Baym - Keldysh) formulation. A classification of diagrams and corresponding resummation in physically meaningful terms is proposed, which considers the finite damping width of all source particles in matter. This way each diagram in this expansion is already free from the infra-red divergences. Both, the correct quasi-particle and quasi-classical limits are recovered from this subset of graphs. Explicit results are given for dense matter in thermal equilibrium. The diagrammatic description may suggest a formulation of a transport theory that includes the propagation of off-shell particles in non-equilibrium dense matter.

¹ permanent address: Moscow Institute for Physics and Engineering, Russia, 115409
Moscow, Kashirskoe shosse 31
Electronic mail: J.Knoll@gsi.de, voskre@rzri6f.gsi.de

1 Introduction

The importance of coherence time effects on the production and absorption of field quanta from the motion of source particles in non-equilibrium dense matter has first been discussed by Landau, Pomeranchuk, Migdal (LPM) [1,2] (and many others later) in the context of bremsstrahlung from ultra-relativistic electrons undergoing multiple rescatterings on Coulomb centers. The first successful measurements of the corresponding suppression of bremsstrahlung have been carried out at the Stanford Linear Accelerator Center very recently [3]. With this paper² we like to supplement some quite intuitive and also formal considerations, which illustrate the nature of production and absorption processes in a dense matter environment. The subject is of quite general nature and applies to many physical problems, where either a source couples weakly to a wave field or for the proper determination of local gain and loss terms in quantum transport. Examples are the production of photon, or di-lepton from a piece of dense nuclear matter or hadron gas formed in high energy nuclear collisions, the gluon or parton radiation and absorption in QCD transport and its practical implementation in parton kinetic models (such problems are discussed, e.g. in [5,6]), the neutrino and axion radiation from supernovas and neutron-star matter (see [7–10]), soft phenomena in quantum cosmological gravity (see [11]), many condensed matter phenomena, as particle transport in metals and semiconductors, radiation in plasma etc. (see [12,13]), and also the decoherence problem in the electro-weak baryogenesis during the early universe (see [14,15]). To be specific, however, we take the example of electrodynamics, considering photon production from a piece of nuclear matter as the source, but when appropriate comment on other cases. Since throughout the paper we discuss the corresponding *proper self energy* of the produced particle, all considerations also apply to gain and loss terms of other particles in non-equilibrium dynamics.

In the context of high-energy nucleus–nucleus collisions [6] for example, it became quite apparent over the last years, that a justification of QCD transport (e.g. in terms of a parton kinetic picture) calls for a proper understanding of all soft processes. Well known is the Rutherford singularity in scattering cross-sections of interactions mediated by the exchange of zero mass quanta (photons/ gluons). In dense matter the exchanged quantum acquires a finite real mass due to Debye-screening. Singularities are also encountered in absorption or radiation processes (bremsstrahlung). Induced by free scattering the rates diverge at vanishing four-momentum q of the radiated quantum, due to the infinite time scales used in the quasi-free approximation. In dense matter, however, due to the *finite free propagation time* τ_{coll} between successive collisions the source particles acquire a *damping* and these rates become regular. In particle physics context, most of the papers on the LPM effect discuss the bremsstrahlung of some fast charged particle, such as hadron, quark or gluon, which traverses a dense hadron gas or quark–gluon plasma, e.g. see refs. [16,5], where the role of the matter is reduced to infinitely massive scatterers. In reality all the particles in dense matter which couple to the radiated field should be treated on

² a brief report of these results is given in [4]

equal footing. Effects of the finite mean free propagation time on photon and gluon radiation have been considered e.g. in refs. [16,18–20,5].

While the problem can be quite simply and intuitively formulated and solved in the classical limit, where a classical source couples to a wave field, e.g. classical charge particles couple to a Maxwell field, considerable conceptual difficulties arise for the very same problem, if the source is described as a quantum many-body system. In fact common standard techniques, like perturbation theory or the quasi-particle approximation (QPA) have serious limitations to describe the production and/or absorption rates over the whole range of energies and momenta, as they completely fail in the soft limit.

Starting from a quantum many-body formulation in terms of Green's functions most derivations of transport descriptions employ two essential approximation steps: i) a gradient expansion and ii) the QPA. For simplicity we concentrate on the defects of the QPA in this paper. In the QPA, which is a consistent approximation scheme for low temperature Fermi liquids (Landau - Migdal, see [21,22]), all particles in the medium are treated *on-shell* with a well determined energy-momentum relation (dispersion relation) which follows from the real part of the retarded self energy of the particle. To be specific in this notion, we use the term "on-shell", when the particle follows a sharp energy-momentum relation. Thus the quasi-particle poles of the retarded Green's function lie just infinitesimally below the causality cut along the real axis in energy. The corresponding approximation scheme in terms of these on-shell states, which have infinite life time, is called quasi-particle approximation (QPA). Due to interactions in dense matter the *damping* of the quasi-particles may become important, the corresponding "quasi-particle" poles of the retarded propagators move into the unphysical sheet below the real axis. As a consequence the mass spectrum of the particles is no longer a sharp delta function but rather acquires a width Γ , and one talks about "off-shell" propagation. In that case one has to leave the standard description in terms of stable single particle states and employ quantum propagators (Green's functions) with continuous mass distributions. Landsmann [23] has coined the notion of "non-shell particles" in this connection. One thus comes to a picture which unifies *resonances* which have already a width in vacuum due to decay modes with the "states" of particles in dense matter, which obtain a width due to collisions (collisional broadening).

The theoretical concepts for a proper many body description in terms of a real time non equilibrium field theory have already been devised by Schwinger, Kadanoff, Baym and Keldysh [24–26] in the early 60^{ies}. First investigations of the quantum effects on the Boltzmann collision term were given by Danielewicz [27], the principle conceptual problems on the level of quantum field theory were investigated by Landsmann [23], while applications which seriously include the finite width of the particles in transport descriptions were carried out only in recent times, e.g. [12,27–37]. For resonances, e.g. the delta resonance in nuclear matter, it was natural to consider broad mass distributions and ad hoc recipes have been invented to include this in transport simulation models. However, many of these recipes are not correct

as they violate some basic principle like detailed balance [34], and the description of resonances in dense matter has to be improved. The present study also gives some hints on how to generalize the transport picture towards the inclusion of off-shell propagations in dense matter [29,32,33].

In this paper we illustrate the practical implications of such non-equilibrium concepts at the example of particle production from the dense matter dynamics. Thus all source particles never reach an asymptotic state and naturally have a continuous mass spectrum. In sect. 2 we derive the basic formulas for the rate of bremsstrahlung. The classical and general quantum mechanical expressions, the latter in terms of non-equilibrium Green's functions and self energies, are derived for the case of non-equilibrium dynamics. In sect. 3 we concentrate on the description of radiation from classical sources. We start with the bremsstrahlung from a classical diffusion process, and subsequently derive the photon spectrum for a classical random walk (Langevin) process in terms of a completely regular multiple collision expansion. The low energy behavior is discussed and pocket correction formulas for the in-matter radiation cross sections are suggested in terms of standard transport coefficients. Also finite size corrections are obtained. Then in sect. 4 we use the non-equilibrium Green's function formalism, see [24–27,38,31], and formulate diagrammatic resummations where all quantities are expressed through physically meaningful terms. We show how infra-red convergent results can be obtained through the account of the finite damping width and discuss the QPA (sect. 4.5) and quasi-classical (QC) (sect. 5) limits from the corresponding infinite series of diagrams. In sect. 6 the lowest order loop diagrams for the production rate from a piece of equilibrium dense matter are analyzed in the quantum case, both at high and low temperatures. Conclusions and perspectives are given in sect. 7. Some formal details are deferred to the Appendix.

We use rational units $\hbar = c = 1$. Whenever the behavior of some quantity is discussed in the classical limit ($\hbar \rightarrow 0$), \hbar will be given explicitly.

2 Basic Formulas for the Rate of Bremsstrahlung

If the source system couples only perturbatively (to lowest order in e^2) to the electromagnetic field, the production or absorption rate of photons can be formulated using standard text book concepts in terms of Fermi's golden rule. The corresponding transition amplitude is given by the electromagnetic current operator between the initial and final states of the source. For dense matter problems it is more advantage to use a more general concept, where the local production and absorption rates are expressed through the current-current correlation function³

³For the description of coordinates and momenta we use the following conventions: numbers 1, 2, etc. abbreviate space-time points $x_1 = (t_1, \mathbf{x}_1)$, etc.; for two-point functions coordinate means are $x = (x_1 + x_2)/2 = (t, \mathbf{x})$, relative coordinates: $\xi = x_1 - x_2 = (\tau, \boldsymbol{\xi})$; the corresponding four vector Wigner coordinates are $(x; q) = (t, \mathbf{x}; \omega, \mathbf{q})$ for the photon and $(x; k) = (t, \mathbf{x}; \epsilon, \mathbf{k})$ for the particles of the source. Whenever advantage or necessary

$$\langle j^{\nu\dagger}(2)j^\mu(1) \rangle \quad \text{for production, and} \quad \langle j^\nu(2)j^{\mu\dagger}(1) \rangle \quad \text{for absorption.} \quad (1)$$

Although $j(x) = j(\mathbf{x}, t)$ is a hermitian operator we distinguish between j and j^\dagger in order to designate the photon creation and annihilation vertex, respectively. The bracket $\langle \dots \rangle$ denotes a quantum ensemble average over the source; quantum states and operators are taken in the Heisenberg picture.

With reference to the description of non-equilibrium systems, where it is advantage to use real-time non-equilibrium field theory concepts, such as the Schwinger - Kadanoff - Baym - Keldysh technique [24–27] we introduce the following notions

$$4\pi \langle j^{\nu\dagger}(2)j^\mu(1) \rangle = -i\Pi^{\mu\nu-+}(1;2), \quad 4\pi \langle j^\nu(2)j^{\mu\dagger}(1) \rangle = -i\Pi^{\nu\mu+-}(2;1), \quad (2)$$

which relate the correlation functions to the proper self energies Π^{-+} and Π^{+-} of the photon, which are responsible for gain and loss (c.f. sect. 4.3). Throughout this paper we use the $\{-, +\}$ notation, defined in detail in sect. 4 in the convention of ref. [38], chapt. 10.

In this formulation the production term for the phase space occupation $n_\gamma(\mathbf{x}, \mathbf{q}, t)$ (Wigner density) of on-shell photons per space-time volume $d^4x = d^3x dt$, and per energy-momentum $\omega - \mathbf{q}$ volume, $d^4q = d\omega d^3q$, with polarization $\eta = \{\eta_\mu\}$ is given by

$$d^8n_\gamma(\mathbf{x}, \mathbf{q}, t) = -i\eta_\mu\eta_\nu\Pi^{\mu\nu-+}(x; q) (1 + n_\gamma(\mathbf{x}, \mathbf{q}, t)) \delta(\omega^2 - \omega_q^2) d^4x d^4q, \quad (3)$$

where ω_q is the photon on-shell energy, and

$$-i\Pi^{\mu\nu-+}(x; q) = 4\pi \int d^4\xi e^{iq\xi} \langle j^{\nu\dagger}(x - \xi/2)j^\mu(x + \xi/2) \rangle \quad (4)$$

denotes the space-time Wigner transformation of the auto correlation function (2). This local gain term is the on-shell version of a general quantum transport concept (Kadanoff-Baym equation [25], c.f. (46), sect. 4). It likewise applies for virtual photons (e.g. dilepton production), replacing the on-shell δ -function in (3) by the corresponding off-shell photon spectral function.

The above expressions are the space and time-dependent version of the more familiar golden rule for quantum transitions between exact stationary eigenstates. Note that by definition, c.f. (4), $-i\eta_\mu\eta_\nu\Pi^{\mu\nu}$ is a real quantity; if integrated over phase-space

we shall swap from one to another or even to some mixed representation, just changing the corresponding arguments of the functions; for space -, or space-time independent systems we drop the argument \mathbf{x} or x , respectively; e.g.: $\Pi_{12} = \Pi(1;2) \leftrightarrow \Pi(x; q) \rightarrow \Pi(\omega, \mathbf{q}) \leftrightarrow \Pi(\tau, \mathbf{q})$; the latter two in space-time homogeneous systems. For simplicity the polarization indices μ and ν or i and k for the spatial part of the tensor structure of $\Pi^{\mu\nu}$ will not always be given in later equations.

volumes $\Delta x \Delta q$ large compared to \hbar it becomes positive and serves as a production rate.

Such a formalism has been applied in many cases employing the QPA for the equilibrium Green's functions, c.f. refs. [41,10]. However, the general formalism allows to go beyond this limit and to account for the finite damping width of the source particles due to their finite mean free path, which is the main topic of this paper.

Therefore the current-current correlation function is the central quantity of interest. In graphical form it is determined by the proper self energy diagram of the photon

$$-i\Pi^{-+} = \text{---} \left(\text{---} \bigcirc \text{---} \right) \text{---} \quad (5)$$

which sums all one-photon irreducible self energy diagrams ⁴. The dashed lines relate to the photon, while the interior area ($-i\Pi$) symbolically denotes the exact inclusion of all strong interactions among the source particles.

2.1 Analytical properties and constraints

The self energies for gain and loss obey some analytical relations that follow right from the definitions (2,4), like

$$-i\Pi^{\mu\nu-+}(1;2) = \left(-i\Pi^{\nu\mu-+}(2;1) \right)^*$$

which implies that $-i\eta_\mu\eta_\nu\Pi^{\mu\nu}(x;q)$ is real. Production and absorption parts obey

$$\Pi^{\mu\nu-+}(x;q) = \Pi^{\mu\nu+-}(x;-q).$$

Integration over ω projects onto equal time properties. Of particular help for the discussion of soft processes [18,19] are the following energy weighted dipole ($\mathbf{q} = 0$) sum-rules (e.g. [39])

$$-i \int_{-\infty}^{\infty} \frac{d\omega}{2\pi} \omega^{n-2} \Pi^{-+}(\omega, \mathbf{q} = 0; t, \mathbf{x}) d^3x = S_n = \begin{cases} 4\pi \langle J^i(t) J^k(t) \rangle & \text{for } n = 2 \\ -2\pi i \langle [D^i(t), J^k(t)] \rangle & \text{for } n = 1 \\ 4\pi \langle D^i(t) D^k(t) \rangle & \text{for } n = 0 \end{cases} \quad (6)$$

which are valid also in the general non-equilibrium case. Here $i, k \in \{1, 2, 3\}$ denote the spatial components. The r.h. expressions are given by the space integrated

⁴To order e^2 naturally all diagrams are one-photon irreducible; however for the application to the production of particles with a larger coupling constant, e.g. for gluons with coupling constant g , also diagrams to higher order in g are relevant and one then has to discard diagrams which are one gluon line reducible.

currents and dipole moments

$$J^i(t) = \int d^3x j^i(t, \mathbf{x}); \quad D^i(t) = \int d^3x x^i j^0(t, \mathbf{x}). \quad (7)$$

While the $n = 2$ sum-rule directly follows from definition (4) and applies to *any* current even non conserving, the other two use current conservation and partial integrations, known as Siegert's theorem (c.f. [40]), and therefore also require that the system has a finite space extension. (If there are no long range correlations, the $n = 2$ and $n = 1$ relations can also be used for infinite matter, if properly taken per volume). For non-relativistic currents the commutator in the $n = 1$ (Thomas - Reiche - Kuhn) sum-rule just becomes the sum of square charges in the system $i[D^i(t), J^k(t)] = \sum e_\nu^2$, where ν labels the constituents.

For systems in *thermal equilibrium* production and absorption follow the detailed balance relation (Kubo - Martin - Schwinger [17])

$$\Pi^{-+}(q; x) = \Pi^{+-}(q; x) e^{-\omega/T} \quad (8)$$

where T is the temperature. They allow to write the l.h.s. of the sum-rules as half-sided integrals, e.g. integrating only the production rate

$$-i \int_0^\infty \frac{d\omega}{2\pi} \omega^{n-2} \Pi^{-+}(\omega, \mathbf{q} = 0; t, \mathbf{x}) \left(1 + (-1)^n e^{\omega/T}\right) d^3x = S_n. \quad (9)$$

These rules have been used to estimate the validity of the quasi-free scattering prescription in kinetic models [18,19]. In the classical limit, where $\hbar\omega \rightarrow 0$ (c.f. sect. 3. below) the l.h.s. of the $n = 1$ and $n = 2$ sum-rules coincide in equilibrium, apart from a factor $T/2$, and the ensuing identity $2S_2 = TS_1$ is a disguised form of the classical equal partition theorem.

A further consistency check for diagrammatic elements which determine the self energy can be given in terms of Ward identities in the case of conserved currents. Since the space-integral of j^0 gives the conserved total charge Z of the system, one may also use that the space integrated density-density correlator is constant in time, i.e.

$$\int d^3x_1 d^3x_2 \Pi^{00-+}(1; 2) = \int d^3x \Pi^{0\nu-+}(\tau, \mathbf{q} = 0; t, \mathbf{x}) = 4\pi Z^2 = \text{const.}, \quad (10)$$

which applies even in non-equilibrium cases. For isolated systems the motion of the center of mass leads to no radiation. Therefore one normally introduces effective charges for the different kind of particles of the source in the standard manner such that the total effective charge vanishes $Z_{eff} = 0$.

3 Radiation from Classical Sources

In this section we discuss two examples which treat the source as a classical system coupled to a Maxwell field. This limit just amounts to evaluate the current-current correlator on the classical level⁵. We discuss the radiation caused by a single charged particle (the source), which stochastically moves in neutral dense matter. The motion of the source is described (a) by mesoscopic transport (diffusion process) and (b) by a microscopic Langevin process. Since these examples represent the QC limits of the corresponding quantum field theory cases, we carry on the discussion in terms of the photon self energy Π^{-+} .

3.1 Diffusion Process

The motion of a non-relativistic source particle is assumed to be described by a time dependent phase-space distribution $f(\mathbf{x}, \mathbf{v}, t)$ in space and velocity with convective current density $\mathbf{j}(\mathbf{x}, t) = e \int d^3v \mathbf{v} f(\mathbf{x}, \mathbf{v}, t)$. For standard dissipative media in equilibrium the velocity autocorrelation function (integrated over space) decays exponentially in time

$$\langle v^i(\tau)v^k(0) \rangle = \frac{1}{3} \langle \mathbf{v}^2 \rangle \delta^{ik} e^{-\Gamma_x |\tau|}, \quad (11)$$

where Γ_x is the relaxation rate which is supposed to be approximately constant on the relaxation time scale $1/\Gamma_x$. It relates to the spatial diffusion coefficient D via Einstein's relation

$$D = \frac{1}{3} \int_0^\infty d\tau \langle \mathbf{v}(\tau)\mathbf{v}(0) \rangle = \frac{1}{3\Gamma_x} \langle \mathbf{v}^2 \rangle. \quad (12)$$

Compared to the infra-red divergent quasi-free result $\propto 1/\omega^2$ (c.f. eq. (28) below) this form of the correlation renders the photon self energy

$$-i\Pi_{\text{cl}}^{-+}(\omega, \mathbf{q} = 0) = 4\pi e^2 \rho_0 \langle v^i v^k \rangle \frac{2\Gamma_x}{\omega^2 + \Gamma_x^2} = 4\pi e^2 \rho_0 \frac{2D\Gamma_x^2}{\omega^2 + \Gamma_x^2} \delta^{ik} \quad (13)$$

regular at four momentum $q = 0$. It is determined by mesoscopic transport properties, namely by the diffusion coefficient D and relaxation rate Γ_x ; ρ_0 is the spatial density of the charged particles.

⁵One has to realize that a classical photon carries no energy in the quantum sense, i.e. $\hbar\omega \rightarrow 0$ and the energy is given by the electromagnetic fields.

Both $f(\mathbf{x}, \mathbf{v}, t)$ and the autocorrelation function can be obtained in closed form, if the time evolution of f , and the propagation of fluctuations δf are governed by a standard (non-relativistic) diffusion process (Fokker–Planck equation)

$$\frac{\partial}{\partial t} f(\mathbf{x}, \mathbf{v}, t) = \left(D\Gamma_x^2 \frac{\partial^2}{\partial \mathbf{v}^2} + \Gamma_x \frac{\partial}{\partial \mathbf{v}} \mathbf{v} - \mathbf{v} \frac{\partial}{\partial \mathbf{x}} \right) f(\mathbf{x}, \mathbf{v}, t). \quad (14)$$

In the equilibrium limit ($t \rightarrow \infty$) the distribution attains a Maxwell-Boltzmann form

$$f_{eq}(\mathbf{x}, \mathbf{v}) = \rho_0 f_{eq}(\mathbf{v}) = \rho_0 (2\pi D\Gamma_x)^{-3/2} \exp \left[-\frac{v^2}{2D\Gamma_x} \right] = \frac{m^3}{(2\pi)^3} e^{-(\epsilon(v)-\mu)/T}, \quad (15)$$

where $T = m \langle \mathbf{v}^2 \rangle / 3 = mD\Gamma_x$ and μ are the equilibrium temperature and chemical potential and $\epsilon(v)$ is the energy of the particle.

At $\tau = 0$ we consider an initial fluctuation $\delta f(\mathbf{x}, \mathbf{v}, \tau = 0) = \delta^3(\mathbf{x})\delta^3(\mathbf{v} - \mathbf{v}_0)$. Its propagation in the equilibrated matter is also governed by the Fokker Planck equation (14). By a Gaussian ansatz for the Fourier transform of this fluctuation $\delta \tilde{f}(\mathbf{q}, \mathbf{y}, \tau) = \int d^3x d^3v f(\mathbf{x}, \mathbf{v}, \tau) \exp[-i\mathbf{q}\mathbf{x} + i\mathbf{y}\mathbf{v}]$ the time-dependence can be obtained in closed form as

$$\begin{aligned} \delta \tilde{f}(\mathbf{q}, \mathbf{y}, \tau) &= \exp \left[-A + i\mathbf{B}\mathbf{y} - C\mathbf{y}^2 \right], \quad \text{where} \\ C &= \frac{D\Gamma_x}{2} \left(1 - e^{-2\Gamma_x\tau} \right), \quad \mathbf{B} = \mathbf{v}_0 e^{-\Gamma_x\tau} - i\mathbf{q}D \left(1 - e^{-\Gamma_x\tau} \right)^2, \\ A &= i\mathbf{q} \int_0^\tau d\tau' \mathbf{B}(\tau') = \frac{Dq^2}{2\Gamma_x} \left[2\Gamma_x\tau - e^{-2\Gamma_x\tau} + 4e^{-\Gamma_x\tau} - 3 \right] - \frac{i\mathbf{q} \cdot \mathbf{v}_0}{\Gamma_x} \left(e^{-\Gamma_x\tau} - 1 \right). \end{aligned} \quad (16)$$

This fluctuation δf is the conditional probability which determines the time-dependence of the current autocorrelation function. With four vectors $\{v^\mu\} = \{1, \mathbf{v}\}$ and $\{B^\mu\} = \{1, \mathbf{B}\}$ one can express the full correlation tensor in the mixed τ, \mathbf{q} representation as

$$\begin{aligned} -i\Pi_{\text{cl}}^{\mu\nu-+}(\tau, \mathbf{q}) &= 4\pi \int d^3x e^{-i\mathbf{q}\mathbf{x}} \langle j^\nu(\mathbf{x}, \tau) j^\mu(\mathbf{0}, 0) \rangle \\ &= 4\pi e^2 \rho_0 \int d^3v f_{eq}(\mathbf{v}) v^\mu B^\nu e^{-A} = 4\pi e^2 \rho_0 \langle v^\mu B^\nu e^{-A} \rangle_{eq} \\ &= 4\pi e^2 \rho_0 \exp \left\{ -\frac{D\mathbf{q}^2}{\Gamma_x} \left(\Gamma_x|\tau| + e^{-\Gamma_x|\tau|} - 1 \right) \right\} \\ &\quad \times \begin{cases} \left\{ \langle v^\mu v^\nu \rangle_{eq} e^{-\Gamma_x|\tau|} - D^2 q^\mu q^\nu \left(e^{-\Gamma_x|\tau|} - 1 \right)^2 \right\} & \text{for } \mu, \nu \in \{1, 2, 3\} \\ iq^\nu D \left(e^{-\Gamma_x|\tau|} - 1 \right) \text{sign}(\tau) & \text{for } \mu = 0, \nu \in \{1, 2, 3\} \\ 1 & \text{for } \mu = \nu = 0 \end{cases} \end{aligned} \quad (17)$$

with A and B as a function of τ , \mathbf{q} and $\mathbf{v}_0 = \mathbf{v}$ from (16). Here the ensemble average $\langle \dots \rangle_{eq}$ over the equilibrium distribution f_{eq} keeps only even moments of \mathbf{v} with $\langle \mathbf{v}^2 \rangle = 3D\Gamma_x$. The result complies exactly with current conservation, i.e. one verifies $\partial_0 \Pi^{0\nu} + iq_k \Pi^{k\nu} \equiv 0$.

For transverse photons terms proportional to $q^\mu q^\nu$ drop. The corresponding spatial part of the tensor is shown in fig. 1, right part. This correlation function decays exponentially as $\sim e^{-\Gamma_x \tau}$ at $\mathbf{q} = 0$, and its width further decreases with increasing momentum $q = |\mathbf{q}|$ due to the increase in spatial resolution. The left part shows the corresponding density-density correlation ($\mu = \nu = 0$), which decays only for non-zero momentum, due to charge conservation.

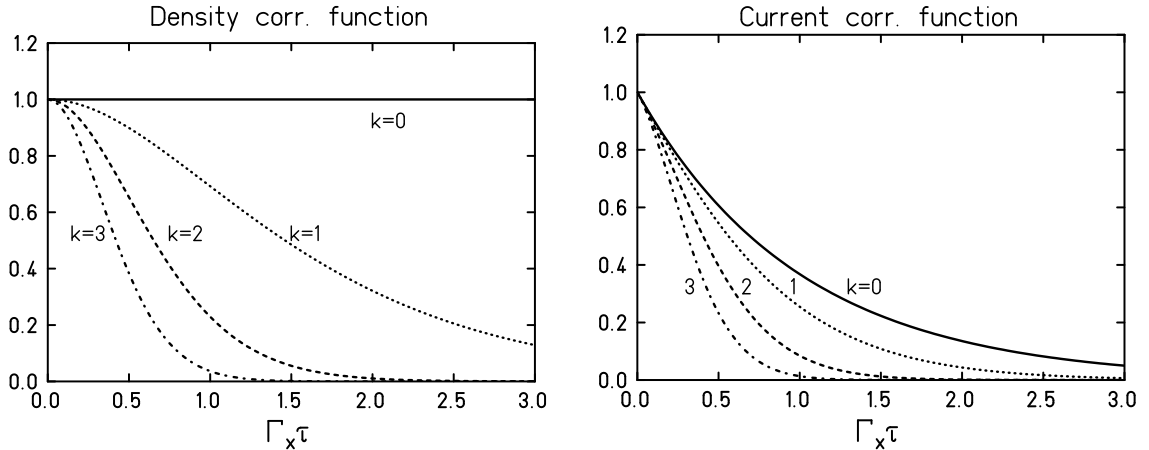


Fig. 1: Density-density and current-current correlation functions, $-i\Pi_{cl}^{00-+}(\tau, \mathbf{q})$ and $-i\Pi_{cl}^{11-+}(\tau, \mathbf{q})$, normalized to the values at $\tau = 0$ as a function of time τ (in units of $1/\Gamma_x$) for different values of the photon momentum $q^2 = 3k^2\Gamma_x^2 / \langle v^2 \rangle$ with $k = 0, 1, 2, 3$.

The remaining time Fourier transformation gives the ω, \mathbf{q} -dependence of the photon self-energy. It can be expressed in terms of the incomplete gamma function. Straightforward expansion in powers $\left\{ (D\mathbf{q}^2/\Gamma_x)e^{-\Gamma_x|\tau|} \right\}^n$ leads to

$$\begin{aligned}
 -i\Pi_{cl}^{-+}(\omega, \mathbf{q}) &= 4\pi e^2 \rho_0 \langle v^i v^k \rangle_{eq} \exp \left[D\mathbf{q}^2/\Gamma_x \right] \\
 &\times \sum_{n=0}^{\infty} \frac{1}{n!} \left(\frac{-D\mathbf{q}^2}{\Gamma_x} \right)^n \frac{2(n+1)\Gamma_x + 2D\mathbf{q}^2}{((n+1)\Gamma_x + D\mathbf{q}^2)^2 + \omega^2}
 \end{aligned} \tag{18}$$

for transverse photons. Since the correlation functions are properly determined from the time structure of the source, they comply with the $n = 2$ (and $n = 1$) sum-rule constraints.

There are two limiting cases where simpler analytical forms can be obtained: i) at small momentum transfers where eq. (18) can be expanded in powers of \mathbf{q} and rewritten as to provide a propagator type form and ii) for large momentum transfers where from the $\exp\{\dots\}$ part in (17) a short time Gaussian behavior emerges. Thus, for small momentum transfers one finds

$$\begin{aligned}
\lim_{\langle v^2 \rangle \mathbf{q}^2 \ll \Gamma_x^2} \left\{ -i\Pi_{\text{cl}}^{-+}(\omega, \mathbf{q}) \right\} &= 4\pi e^2 \rho_0 \langle v^i v^k \rangle_{\text{eq}} \frac{2\Gamma_x}{\Gamma_x^2 + \omega^2 + \frac{2\Gamma_x^2 - 4\omega^2}{3(4\Gamma_x^2 + \omega^2)} \langle v^2 \rangle \mathbf{q}^2} \\
&\approx 4\pi e^2 \rho_0 \langle v^i v^k \rangle_{\text{eq}} \frac{2\Gamma_x}{\Gamma_x^2 + \omega^2 + \langle v^2 \rangle \mathbf{q}^2 / 6} \quad \text{for } \omega \ll \Gamma_x
\end{aligned} \tag{19}$$

which generalizes the relaxation result (11,13) to finite \mathbf{q} . On the other hand for large momenta one realizes that

$$\begin{aligned}
\lim_{D \mathbf{q}^2 \gg \Gamma_x} \left[-i\Pi_{\text{cl}}^{-+}(\tau, \mathbf{q}) \right] &= 4\pi e^2 \rho_0 \langle v^i v^k \rangle_{\text{eq}} \exp \left[-D \mathbf{q}^2 \Gamma_x \tau^2 / 2 \right], \quad \text{and therefore} \\
\lim_{D \mathbf{q}^2 \gg \Gamma_x} \left[-i\Pi_{\text{cl}}^{-+}(\omega, \mathbf{q}) \right] &= 4\pi e^2 \rho_0 \langle v^i v^k \rangle_{\text{eq}} \sqrt{\frac{2\pi}{D \mathbf{q}^2 \Gamma_x}} \exp \left\{ -\frac{\omega^2}{2D \mathbf{q}^2 \Gamma_x} \right\} \\
&= 4\pi e^2 \langle v^i v^k \rangle_{\text{eq}} \frac{m^2 T}{2\pi |\mathbf{q}|} \exp \left\{ -\left(\frac{m}{2} \omega^2 / |\mathbf{q}|^2 - \mu \right) / T \right\},
\end{aligned} \tag{20}$$

where obviously the essential contributions come from velocities which satisfy the Cherenkov condition $|\mathbf{v}| \approx \omega / |\mathbf{q}|$. This limit is independent of the relaxation rate Γ_x and coincides with the quantum one-loop diagram result in the corresponding large $|\mathbf{q}|$ limit, as we shall see in sect. 6.

Although the above expressions give the exact solution of the mathematical problem posed in this section, its physical interpretation has to be done with some care for the following reason. The equilibrium source distribution contains velocity components that exceed the speed of light. Therefore for the physical result mistakes of the order of $\exp[-3/(2\langle v^2 \rangle)] = \exp[-m/(2T)]$ are expected. This restricts the application to non-relativistic sources and for large \mathbf{q} to space-like photons, where $|\mathbf{q}| \gg \omega$.

For systems with given fixed mean-square velocity $\langle v^2 \rangle = \text{const.}$ the exact classical on-shell rate (3) at $|\mathbf{q}| = \omega$ evidently scales as a function of ω / Γ_x . It properly vanishes at $\omega = 0$ and at infinity. It is important to note that the rate has an upper bound of $\approx \frac{2}{3\pi} e^2 \rho_0 \langle v^2 \rangle$, and indeed attains its maximum value around $\omega \approx \Gamma_x$, which is collision-rate independent. For simplicity we quote the closed form obtained in the non-relativistic limit (19), which coincides with the dipole limit. There

$$\frac{d^5 n_\gamma}{d^3 x d\omega dt} \approx \frac{4}{3\pi} e^2 \rho_0 \langle v^2 \rangle \frac{\omega / \Gamma_x}{1 + (\omega / \Gamma_x)^2} \rightarrow \frac{4}{3\pi} e^2 \rho_0 \langle v^2 \rangle \begin{cases} \Gamma_x / \omega & \text{for } \omega \gg \Gamma_x \\ \frac{1}{2} & \text{for } \omega = \Gamma_x \\ \omega / \Gamma_x & \text{for } \omega \ll \Gamma_x. \end{cases} \tag{21}$$

One realizes that the ultra-violet part of the spectrum $\omega \gg \Gamma_x$ behaves as intuitively expected, fig. 2: the rate grows proportional to the relaxation rate, until it saturates around $\omega \approx \Gamma_x$. For the soft part $\omega \ll \Gamma_x$, however, the rate becomes inversely proportional to the collision rate! The higher the collision rate the more suppressed the spectrum. In order to illustrate the non-perturbative character of this soft behavior supposes $\Gamma_x \propto g^2$, where g is the strong coupling constant of the source

system. One sees that indeed the low- ω part with $\Pi \propto e^2\omega/\Gamma_x \propto e^2\omega/g^2$ represents a genuine non-perturbative result in g , while the large ω -part, where $\Pi \propto e^2g^2/\omega$, is well described perturbatively.

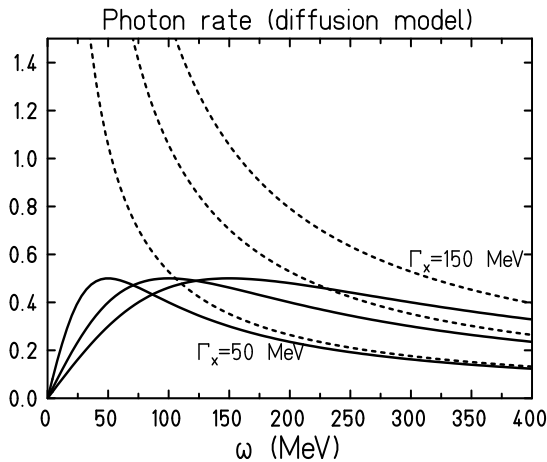


Fig. 2: Rate of real photons $dN/(d\omega dt)$ in units of $4\pi e^2 \langle v^2 \rangle / 3$ for a non-relativistic source for $\Gamma_x = 50, 100, 150$ MeV; for comparison the IQP results (dashed lines) are also shown.

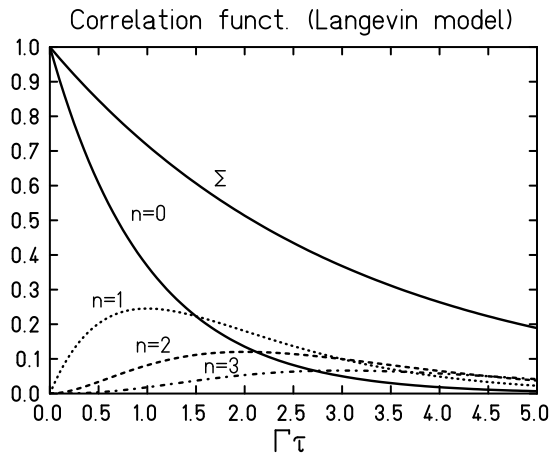


Fig. 3: Current correlation function for the first terms $n = 0, 1, 2, 3$ of the Langevin result, eq. (22) and the total sum (Σ) for the case that $\Gamma_x/\Gamma = \langle (\mathbf{v}_m - \mathbf{v}_{m+1})^2 \rangle / (2 \langle v^2 \rangle) = 1/3$.

3.2 Microscopic Langevin Process

For a later comparison with quantum diagrams in sect. 4 we should look into the corresponding microscopic picture of classical propagation. There one can consider a classical random process (Langevin process), where hard scatterings occur at random with a constant mean collision rate Γ . These scatterings consecutively change the velocity of a point charge from \mathbf{v}_m to \mathbf{v}_{m+1} to \mathbf{v}_{m+2}, \dots (in the following subscripts m, n , and l refer to the collision sequence, while superscripts $i, k \in \{1, 2, 3\}$ specify the spatial components of vectors and the self-energy tensor). In between scatterings the point charge moves freely. For such a multiple collision process some explicit results can be given. They all refer to the case of vanishing photon momentum $\mathbf{q} = 0$ (dipole approximation) and therefore apply to non-relativistic sources where $\langle v^2 \rangle \mathbf{q}^2 \ll \Gamma_x^2$ or to dilepton production, for example, since only the time structure is well known in this case, while the space structure would require an integration of the random classical paths.

For such a Langevin process the modulus of the autocorrelation function takes a simple Poissonian form (fig. 3)

$$\begin{aligned}
 -i\Pi_{\text{cl}}^{-+}(\tau, \mathbf{q} = 0) &= 4\pi e^2 \rho_0 \langle v^i(\tau) v^k(0) \rangle \\
 &= 4\pi e^2 \rho_0 e^{-|\Gamma\tau|} \sum_{n=0}^{\infty} \frac{|\Gamma\tau|^n}{n!} \langle v_m^i v_{m+n}^k \rangle_m .
 \end{aligned} \tag{22}$$

Here $\langle \dots \rangle_m$ denotes the average over the discrete collision sequence $\{m\}$. This form, which one writes down intuitively, directly includes what one calls *damping* and therefore corresponds to a resummation description in the quantum case. The corresponding perturbation theory result is obtained through an expansion in powers of Γ

$$-i\Pi_{\text{cl}}^{-+}(\tau, \mathbf{q} = 0) = 4\pi e^2 \rho_0 \sum_{n=0}^{\infty} \frac{|\Gamma\tau|^n}{n!} \sum_{l=0}^n (-1)^k \binom{n}{l} \langle v_m^i v_{m+l}^k \rangle_m, \quad (23)$$

which for dimensional reasons is also a power series in $|\tau|$ in this case. If the $\langle v_m^i v_{m+n}^k \rangle$ expectation values are replaced by unity in (22) or (23), one obtains the 00-component of Π which becomes constant in time in line with (10).

The time Wigner transform of (22) determines the ω -spectrum at vanishing \mathbf{q}

$$-i\Pi_{\text{cl}}^{-+}(\omega, \mathbf{q} = 0) = 4\pi e^2 \rho_0 \sum_{n=0}^{\infty} \langle v_m^i v_{m+n}^k \rangle_m \operatorname{Re} \left\{ \frac{2\Gamma^n \{(\Gamma + i\omega)^{n+1}\}}{(\omega^2 + \Gamma^2)^{n+1}} \right\}. \quad (24)$$

This is a genuine *multiple collision* description for the photon production rate in completely regular terms due to the $(\omega^2 + \Gamma^2)^n$ form of all denominators. Each term is regular, since right from the beginning one accounts for the damping of the source particle because of its finite mean time $1/\Gamma$ between collisions. The result (24) still accounts for the *coherence* of the photon field, now expressed through the correlations $\langle \mathbf{v}_m \mathbf{v}_{m+n} \rangle_m$ arising from the sequence of collisions. Note in particular, that, although the total expression is positive, the $n > 0$ terms can be negative since they describe the interference of the radiation arising from different propagation segments of the source particle. Thus, the terms in (24) define partial rates, which later (sect. 5.2) will be associated with specific self energy diagrams.

As already mentioned, the \mathbf{q} -dependence of the self energy cannot be given in closed form in general apart from the $n = 0$ term (c.f. with $n = 0$ term from eq. (24))

$$-i\Pi_{\text{cl}}^{-+}(\omega, \mathbf{q}) \approx 4\pi e^2 \rho_0 \left\langle \frac{2\Gamma v_m^i v_m^k}{(\omega - \mathbf{q}\mathbf{v})^2 + \Gamma^2} \right\rangle_m. \quad (25)$$

It shows the typical Cherenkov enhancement at $\omega = \mathbf{q}\mathbf{v}$. At this level one may be tempted to associate this ($n = 0$) term with the relaxation ansatz result (13). This however is only true if $\langle \mathbf{v}_m \mathbf{v}_{m+n} \rangle_m = 0$ for $n \neq 0$, an approximation recently used in refs. [16]. In the general case velocity correlations between successive scatterings exist, and there will be a difference between the microscopic mean collision rate Γ and the mesoscopic relaxation rate Γ_x . Still, for systems, where the velocity is degraded by a constant fraction α per collision, such that $\langle \mathbf{v}_m \cdot \mathbf{v}_{m+n} \rangle_m = \alpha^n \langle \mathbf{v}_m \cdot \mathbf{v}_m \rangle_m$, one can resum the whole series in (24) and thus recover the relaxation result (13) at $\mathbf{q} = 0$. The macroscopic rate Γ_x is then determined by the microscopic scattering

properties through $\Gamma_x = (1 - \alpha)\Gamma$, or $2 \langle (\mathbf{v}_m)^2 \rangle_m \Gamma_x = \langle (\mathbf{v}_m - \mathbf{v}_{m+1})^2 \rangle_m \Gamma$. This clarifies that the diffusion result (18) represents a resummation of the random multiple collision result.

The following relations show different reformulations and limits of the Langevin result (24). For instance the invariance of (24) is not directly visible, since absolute velocities enter. Still the perturbation expression (23) can be rewritten, such that except for the zero order term, which drops out in the Fourier transform, only velocity differences appear

$$-i\Pi_{\text{cl}}^{-+}(\tau, \mathbf{q} = 0) = 4\pi e^2 \rho_0 \left\{ \langle v_m^i v_m^k \rangle_m - \frac{|\Gamma\tau|}{2} \langle (v_m^i - v_{m+1}^i)(v_m^k - v_{m+1}^k) \rangle_m \right. \\ \left. - \sum_{n=2}^{\infty} \frac{|\Gamma\tau|^n}{n!} \sum_{l=0}^{n-2} (-1)^k \binom{n-2}{l} \langle (v_m^i - v_{m+1}^i)(v_{m+l+1}^k - v_{m+l+2}^k) \rangle_m \right\}. \quad (26)$$

Terms of lowest odd order in $|\tau|$ determine the asymptotic large ω (ultra violet) behavior of the spectrum

$$\lim_{\omega \rightarrow \infty} [-i\Pi_{\text{cl}}^{-+}(\omega, \mathbf{q} = 0)] = \frac{4\pi e^2 \rho_0}{\Gamma} \left\{ \frac{\Gamma^2}{\omega^2} \langle (v_m^i - v_{m+1}^i)(v_m^k - v_{m+1}^k) \rangle_m \right. \\ \left. + \sum_{n=2}^{\infty} \left(\frac{\Gamma}{\omega}\right)^{2n} \sum_{l=0}^{2n-3} (-1)^l \binom{2n-3}{l} \langle (v_m^i - v_{m+1}^i)(v_{m+l+1}^k - v_{m+l+2}^k) \rangle_m \right\}. \quad (27)$$

Apart from the mean collision time $\approx 1/\Gamma$ this is an expansion in powers of $(\Gamma/\omega)^2$ and therefore represents the perturbation expansion result for the classical source (Γ representing the interaction, while $1/\omega$ relates to the intermediate propagator). This perturbation expansion (27) is interesting since it already displays the main problem: While for $\omega \gg \Gamma$ the series converges, if higher order correlations cease sufficiently fast, there is no hope to ever recover the correct result (24) for $\omega \ll \Gamma$. This is so, since i) this series is necessarily divergent (it has to recover $1/(\omega^2 + \Gamma^2)$ by a power series in Γ), but also it misses the knowledge on the even powers in τ in eq. (26) which essentially determine the soft behavior.

The first term in (27) represents the *incoherent quasi-free* production rate which for finite \mathbf{q} at given polarization η reads

$$-i\eta_\mu \eta_\nu \Pi_{\text{IQF}}^{\mu\nu-+}(\omega, \mathbf{q}) = 4\pi e^2 \rho_0 \Gamma \left\langle \left| \frac{\eta k_m}{q k_m} - \frac{\eta k_{m+1}}{q k_{m+1}} \right|^2 \right\rangle_m. \quad (28)$$

It carries the known divergence at the soft point $q = 0$, c.f. dashed lines in fig. 2 and 4. In conclusion: *the commonly used IQF prescription fails for soft particle production.*

3.3 Finite Size Corrections

For systems of finite spatial extension and conserved currents one can consider the $n = 0$ sum rule. It demands that $\Pi^{\mu\nu-+}(q; x)$ has to vanish at least quadratically with $q \rightarrow 0$. This property survives in the classical limit, where formally $\hbar \rightarrow 0$ and the spectrum becomes continuous. Thus, the term of zero order in ω given by $\int_{-\infty}^{\infty} \langle (\mathbf{v}(\tau))(\mathbf{v}(0)) \rangle d\tau$ has to drop and the ensuing low energy part of the spectrum (24) starts quadratically in ω

$$\lim_{\omega \rightarrow 0} \left[-i\Pi_{\text{cl}}^{-+}(\omega, \mathbf{q} = 0) \right] = -\frac{4\pi e^2 \rho_0}{\Gamma} \left\{ \frac{\omega^2}{\Gamma^2} \sum_{n=0}^{\infty} (n+1)(n+2) \langle v_m^i v_{m+n}^k \rangle_m + \mathcal{O}\left(\frac{\omega^4}{\Gamma^4}\right) \right\}. \quad (29)$$

The simple relaxation ansatz (11) does not fulfill this finite size condition, since it ignores long term anti-correlations on the scale of some recurrence time $1/\Gamma_{rec}$. That is the time, where on the mean the center of charges returns to the same point⁶. This defect of the relaxation ansatz may be cured by a more general form which includes such an anti-correlation, e.g.

$$\begin{aligned} \langle \mathbf{v}(\tau) \mathbf{v}(0) \rangle &= \langle \mathbf{v}^2 \rangle \left\{ e^{-\Gamma_x |\tau|} - \frac{\Gamma_{rec}^2}{\Gamma_x} |\tau| e^{-\Gamma_{rec} |\tau|} \right\}; \\ -i\Pi_{\text{cl}}^{-+}(\omega, \mathbf{q} = 0) &= 4\pi e^2 \rho_0 \langle v^i v^k \rangle \frac{2}{\Gamma_x} \left\{ \frac{\Gamma_x^2}{\omega^2 + \Gamma_x^2} + \frac{\Gamma_{rec}^2 (\omega^2 - \Gamma_{rec}^2)}{(\omega^2 + \Gamma_{rec}^2)^2} \right\}. \end{aligned} \quad (30)$$

The extra parameter Γ_{rec} can be determined such that the spectrum fulfills the $n = 0$ dipole sum-rule (6). For larger systems one infers that $\Gamma_{rec} \approx 2 \langle v^2 \rangle / (\langle x^2 \rangle \Gamma_x)$, where $\langle x^2 \rangle$ is the mean-square extension.

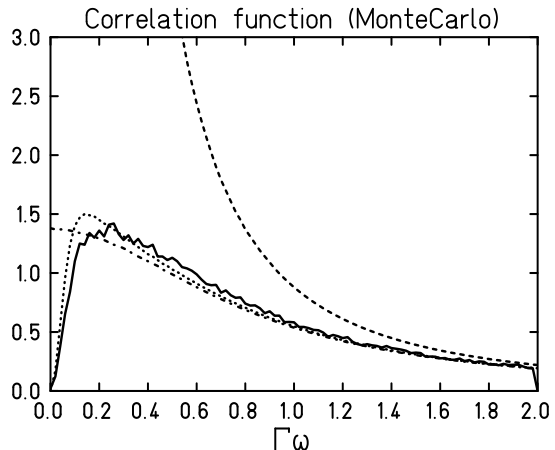
For small systems both time scales become comparable and the self energy tensor attains the form

$$-i\Pi_{\text{cl}}^{-+}(\omega, \mathbf{q} = 0) = 4\pi e^2 \rho_0 \langle v^i v^k \rangle \frac{4\Gamma_x \omega^2}{(\omega^2 + \Gamma_x^2)^2} \quad \text{for} \quad \Gamma_x = \Gamma_{rec}. \quad (31)$$

This form has been found in the one-dimensional model of ref. [19], where due to the dominance of back scattering both time scales merge.

⁶ not to be confused with the Poincare recurrence time, which is of no relevance here.

Fig. 4: Current correlation function $-i\Pi^{11-+}(\omega, \mathbf{q} = 0)$ for a random collision sequence limited to a finite size in space such that $\langle x^2 \rangle \simeq 10 \langle v^2 \rangle / \Gamma^2$ and $\Gamma_x = 0.8\Gamma$: full line from Monte Carlo calculation of the phase integral (32); dashed-dotted line from the analytic Langevin result (24); dotted line includes finite size corrections (30); dashed line from quasi-free scattering prescription.



3.4 Comparison with Monte Carlo Evaluation of Amplitudes

For illustration we like to present a simple model result and compare it to a Monte Carlo method, where amplitudes are calculated by considering the phase of the photon field along the classical orbits. Thus, one evaluates

$$\int dt \mathbf{v}(t) \exp[i\omega t - i\mathbf{q}\mathbf{x}(t)] \quad (32)$$

along the random straight sections of the classical paths in the cascade model. This method also permits to illustrate the finite size corrections discussed above. The dotted line in fig. 4. shows the Monte Carlo phase integral result (32) from an oriented random walk, compared to the simple relaxation result (13), dashed line. The example has the property that the motion is limited to a finite space with $\langle x^2 \rangle \simeq 10 \langle v^2 \rangle / \Gamma^2$ and $\Gamma_x = 0.8\Gamma$. The sharp dip at $\omega = 0$ and the little overshoot around $\omega \sim 0.3\Gamma$ are due to the finite size of the system. The full line gives the relaxation result including the finite size corrections (30).

Evidently the Monte Carlo method is highly unreliable due to the strong cancellations of terms that are randomly generated. The precision in fig. 4 is obtained with 200 cascade runs where each path has about 10^3 collisions (simulation codes have by far less statistics!). The analytical result (24) has significant computational advantages, provided the random process is of this form. For the same precision already a single representative path with about 10^3 collisions is sufficient, while for the relaxation ansatz one only has to determine the relaxation rate, i.e. a simple moment in time.

3.5 Infra-red Divergences, Current Conservation, Gauge Invariance and Identities

In the above multiple collision description *with damping* (22) all terms have a finite range in time. Thus, they all are void of infra-red divergences and so is any limited sum of terms of them. This is the desirable feature that we are aiming at. In addition

the example above illustrates that in many cases only a few rescattering terms are necessary in order to properly recover the correct result for the transverse part of the correlation tensor both at small and large ω . In fact the number n_x of required rescattering terms is given by $n_x \sim \Gamma/\Gamma_x$.

The picture is more subtle for the longitudinal components of the tensor, since some particular integrals are conserved (time independent) as they related to the total charge, c.f. eq. (10), sect. 2.1. Thus $-i\Pi^{00+}(\mathbf{q} = 0, \tau)$, c.f. fig. 1, has to be constant. For the Langevin case this identity holds, since

$$\sum_{n=0}^{\infty} \frac{(\Gamma\tau)^n}{n!} e^{-\Gamma\tau} \equiv 1. \quad (33)$$

However, for any finite number of such terms this identity can never be recovered exactly for all times, since the relaxation time of total charge is infinite!

Quite often one is interested in a solution of the problem up to a maximal time t_{max} , and one likes to request charge conservation on the correlator level to be maintained only within this time span or within the corresponding ω -range limited to $\omega > \omega_{min} = 1/t_{max}$. With this limitation a finite number of terms $n_x \sim \Gamma t_{max} \sim \Gamma/\omega_{min}$ is required for a proper description also of the longitudinal parts of the correlation tensor at $\mathbf{q} = 0$.

The above features have to be contrasted with perturbation theory (c.f. eq. (23)), where the correlation function can be expressed by a power series in Γ in this case and therefore leads to a power series in τ . Here the zero order term is finite (and trivially constant in time), while the higher order terms cancel out for each given order, c.f. (23). Thus, in perturbation theory current conservation is maintained order by order also for the classical correlator (as one is used to from the quantum case). The price to be payed is that in perturbation theory the infra-red properties are completely ill.

In favor of the finite width description one should realize that *any finite width calculation up to a certain order n_x includes the perturbation theory or QPA results up to the very same order n_x* . In other words, if one would expand all finite width terms within the order n_x into powers of Γ one recovers all the QPA or perturbation theory terms up to that order!

Only in the above sense current conservation, gauge invariance and other identities related to them (e.g. Ward identities) can be understood and expected to hold for a finite set of terms. These considerations are general. In particular they also apply to any finite set of self-energy diagrams in the quantum case, which use full Green's functions with *damping* as discussed in the next section.

This completes the formal discussion of the classical radiation rate and the corresponding classical expressions for the self energy of the photon.

4 Non Equilibrium Green's Function Description

In this section the production rate or photon self energy (2) is discussed in the context of non-equilibrium quantum field theory, in terms of Green's functions and the corresponding non-equilibrium diagrams. Thereby one has to go beyond perturbation theory which is not applicable for strongly interacting systems. The idea to formulate theory in terms of appropriately defined physical terms was very fruitful. It resulted in the development of the QPA method, see [21,22], where the changes in the real part of the fermion self energy are taken into account substituting the free particle energy $\epsilon_{\mathbf{p}}^0$ by the corresponding QPA energy. This method proved to be very successful for the case of equilibrium matter at rather small temperature ($T \ll \epsilon_F$, where ϵ_F is the Fermi energy), since higher order corrections lead to additional $(T/\epsilon_F)^2$ factors [41].

Since in the QPA the imaginary part of the self energy ($\text{Im}\Sigma_F^R$) is supposed to be negligible in the corresponding Green's functions it still suffers the same infra-red problems as the perturbation expansion. Any finite set of diagrams leads to infra-red divergences in the soft limit ($q \rightarrow 0$). Even certain resummation methods as the hard thermal loop expansion [42,43] in QCD do not cure the problem. On the other hand the classical considerations of the previous section clarify, that all infra-red divergences disappear, if one properly accounts for the finite collision rate Γ . Thus, one has to avoid the zero-width perturbation theory or QPA and seriously account for the finite damping width $\Gamma = -2\text{Im}\Sigma^R$ of the source particles.

Therefore the simplest and physically most meaningful step is to go to the *full* Green's functions \mathbf{G} (full lines in diagrams) associated with the in-medium propagation for the constituents of the source. Thus one has to solve Dyson's equation in order to include also the damping width of the particles. This is done in sect. 4.2. The derivation of transport schemes is summarized. Further on some physically meaningful resummations of the diagrams are proposed. Various graphical contributions to the self energy diagram (5) are discussed in the QPA, and in the QC limit.

4.1 Vertices and Green's functions

For a theory of fermions interacting with bosons the basic diagrammatic elements are the corresponding Green's functions iG (lines) and interaction vertices $-iV$. For non equilibrium description it makes no sense to discuss amplitudes. Rather one evaluates the time-dependence of the ensemble averaged expectation values of observables. Such expectation values involves standard time-ordered products (\hat{T}) for the evolution of the "ket" $| \rangle$ and also anti-time ordered products (\hat{A}) for the evolution of the "bra" $\langle |$ in the matrix elements. Both can be summarized to a contour-ordered product [24]. Therefore one distinguishes two types of vertices: the $(-)$ vertices with value $-iV$ pertain to the time ordered part, and the adjoint $(+)$

vertices with value $+iV$ for the anti-time ordered section, in the here used convention[38]. Thereby V is the real interaction vertex of the Lagrangian. Correspondingly two point functions, like the Green's functions, have four components, which can be arranged in matrix form (we reserve bold face notation for the two by two $\{-+\}$ matrices)

$$i\mathbf{G}_{12} := \begin{pmatrix} iG_{12}^{--} & iG_{12}^{-+} \\ iG_{12}^{+-} & iG_{12}^{++} \end{pmatrix} = \begin{pmatrix} \langle \hat{\mathbf{T}}\Psi(1)\Psi^\dagger(2) \rangle & \mp \langle \Psi^\dagger(2)\Psi(1) \rangle \\ \langle \Psi(1)\Psi^\dagger(2) \rangle & \langle \hat{\mathbf{A}}\Psi(1)\Psi^\dagger(2) \rangle \end{pmatrix} \quad (34)$$

Here 1 and 2 denote the two space-time points and $\langle \dots \rangle$ the ensemble average. Upper and lower signs refer to fermion and boson Green's functions, respectively. The four Green's function components are obviously not independent. Rather they relate to the retarded and advanced ones by

$$\begin{aligned} G^R &:= -i \left\langle \left[\Psi(1), \Psi^\dagger(2) \right]_{\pm} \right\rangle \Theta(t_1 - t_2) = G^{--} - G^{-+} = G^{+-} - G^{++} \\ G^A &:= +i \left\langle \left[\Psi(1), \Psi^\dagger(2) \right]_{\pm} \right\rangle \Theta(t_2 - t_1) = G^{--} - G^{+-} = G^{-+} - G^{++}, \end{aligned} \quad (35)$$

where Θ is the step function and $[\dots, \dots]_{\pm}$ denotes the fermion anti- or boson commutator.

The unperturbed Green's function \mathbf{G}_{12}^0 is resolvent of the corresponding free single particle Schrödinger - (non rel. fermions) or Klein-Gordon equation (rel. bosons)

$$S_1 \mathbf{G}_{12}^0 = (S_2)^* \mathbf{G}_{12}^0 = \delta(1-2) \boldsymbol{\sigma}_z, \quad S = \begin{cases} i\partial_t + \frac{\Delta}{2m} & \text{(non rel. F)} \\ -\partial_t^2 + \Delta - m^2 & \text{(rel. B)} \end{cases} \quad (36)$$

where the subscript specifies the coordinate to differentiate. Here $\boldsymbol{\sigma}_z$ is the third Pauli matrix and $\delta(1-2)$ is the four-space delta function.

With this extension to the two types of vertices $-$ and $+$ and the corresponding four Green's function components all standard diagrammatic Feynman rules defined for amplitudes can directly be generalized. These rules are then again defined with respect to the *real time* (as in zero temperature theory)⁷. For conventions and a detailed explanation of the *diagrammatic rules* used here we refer to the text book of Lifshitz and Pitaevskii [38]. For a given n -point function all n external vertices have a specified sign assignment, while one has to sum over all possible sign combinations at the internal vertices.

⁷ Please note that in refs. [24,25,27] the diagrammatic rules are defined with respect to the closed time contour, which leads to the same definition for Green's functions, however the off-diagonal components of the self energies used there $\Sigma^< = -\Sigma^{-+}$ and $\Sigma^> = -\Sigma^{+-}$ have opposite values.

4.2 Resummations: Dyson - and Kadanoff-Baym equations

Since diagrammatic elements, e.g. Green's functions G and self energies Σ are connected at a given vertex, the same vertex type – or + appears in both functions and Dyson's equation can simply be written in matrix form

$$\mathbf{G}_{12} = \mathbf{G}_{12}^0 + \int d3d4 \mathbf{G}_{13}^0 \mathbf{\Sigma}_{34} \mathbf{G}_{42} \quad \text{or simply as} \quad (37)$$

$$\mathbf{G} = \mathbf{G}^0 + \mathbf{G}^0 \odot \mathbf{\Sigma} \odot \mathbf{G} = \mathbf{G}^0 + \mathbf{G} \odot \mathbf{\Sigma} \odot \mathbf{G}^0$$

involving usual matrix algebra, which automatically provides the sum over all internal vertex sign combinations. Here the two by two matrix $\mathbf{\Sigma}$ denotes the proper self energy of the source particles⁸. The \odot abbreviates the space-time folding. In diagrams Dyson's equation becomes

$$\begin{aligned} \text{---} &= \text{---} + \text{---} \text{---} \text{---} \\ \text{~~~~} &= \text{~~~~} + \text{~~~~} \text{---} \text{~~~~} \end{aligned} \quad (38)$$

where we explicitly distinguish between fermions (label F ; full straight lines for \mathbf{G}_F) and bosons (label B ; full wavy lines for \mathbf{G}_B). The four components of $-i\mathbf{\Sigma}$ are defined as the sum of all standard proper self energy diagrams like in normal perturbation theory, now however with definite + or – assignments at the external vertices, and summed over the $-+$ signs at all internal vertices as explained above.

Using the resolvent properties (36) of \mathbf{G}^0 one can transform Dyson's equation into a set of integro-differential equation which in short matrix notation reads

$$\begin{aligned} S_1 \mathbf{G}_{12} &= \delta(1-2) \boldsymbol{\sigma}_z + \boldsymbol{\sigma}_z \int d3 \mathbf{\Sigma}_{13} \mathbf{G}_{32} \\ (S_2)^* \mathbf{G}_{12} &= \delta(1-2) \boldsymbol{\sigma}_z + \int d3 \mathbf{G}_{13} \mathbf{\Sigma}_{32} \boldsymbol{\sigma}_z \end{aligned} \quad (39)$$

The four equations involving the time changes of G^{-+} and G^{+-} are known as the Kadanoff-Baym equations [25], originally derived by the imaginary time method. Here they are a direct consequence of the Dyson equation in matrix form. Like the four components of \mathbf{G} also those of $\mathbf{\Sigma}$ are not independent. Their dependence can be determined observing that the Dyson equations for retarded or advanced Green's

⁸ We reserve $\mathbf{\Sigma}$ for the self energy of the source particles, while $\mathbf{\Pi}$ denotes the self energy of the external photon.

functions have to involve only retarded or advanced entities, respectively. Thus they completely decouple

$$G^R = G^{0R} + G^{0R} \odot \Sigma^R \odot G^R, \quad G^A = G^{0A} + G^{0A} \odot \Sigma^A \odot G^A, \quad (40)$$

where Σ^R and Σ^A are the corresponding advanced and retarded self energies. From (35), (37) and (40) one therefore follows that

$$\Sigma^R = \Sigma^{--} + \Sigma^{-+}, \quad \Sigma^A = \Sigma^{--} + \Sigma^{+-}, \quad \Sigma^{++} + \Sigma^{--} = -(\Sigma^{+-} + \Sigma^{-+}). \quad (41)$$

The full Green's functions account for the finite damping width

$$\Gamma = -2\text{Im}\Sigma^R = i(\Sigma^{-+} - \Sigma^{+-}) \quad (42)$$

of the particles, which destroys the sharp relation between energy and momentum. Thus the spectral function

$$A(x; p) := -2\text{Im}G^R(x; p) = i(G^{+-}(x; p) - G^{-+}(x; p)) \quad (43)$$

is no longer an on-shell δ -function but rather has a width $\Gamma(x; p)$. This width does not only arise from decays (resonances) but also from collisions of the particles in dense matter. It is important to realize, that the resummation to full Green's functions (bold straight or wave lines in diagrams) reduces the set of all diagrams to a subset of diagrams with *skeleton topology*, where all self energy insertions are excluded in the diagrams.

4.3 Transport equations

In the presented picture the Wigner transforms of the off-diagonal Green's functions $\mp iG^{-+}$ and iG^{+-} are *Wigner densities in four space and four momentum* for the *occupied* and *available* 'single particle states', which now have a finite width and therefore can be *off* mass shell. We will see that the corresponding non-diagonal components of the proper self energy $-i\Sigma$ are the gain and loss coefficients for the transport description of these Wigner densities.

The entry to such transport equations is given by the Kadanoff-Baym equations, which are contained in the set (39). Subtracting the two equations for G^{-+} yields

$$\left. \begin{aligned} & \left(i(\partial_{t_1} + \partial_{t_2}) + \frac{\Delta_1 - \Delta_2}{2m} \right) \\ & \left(-\partial_{t_1}^2 + \partial_{t_2}^2 + \Delta_1 - \Delta_2 \right) \end{aligned} \right\} G_{12}^{-+} \quad (44)$$

$$= \int d\mathbf{3} \left\{ \Sigma_{13}^{--} G_{32}^{++} + \Sigma_{13}^{-+} G_{32}^{++} + G_{13}^{--} \Sigma_{32}^{-+} + G_{13}^{-+} \Sigma_{32}^{++} \right\}$$

for non rel. fermion or rel. bosons, respectively. The next step is to take the Wigner transformation of this equation. This involves the Wigner transformation of convolution integrals $C(1;2) = \int d\mathbf{3} A(1;3)B(3;2)$ which formally can be obtained through

$$\begin{aligned} C(x;k) &= \exp\left[\frac{i}{2}(\partial_k^A \partial_x^B - \partial_x^A \partial_k^B)\right] A(x;k) B(x;k) \\ &\simeq A(x;k) B(x;k) + \frac{i}{2} \{A, B\}, \end{aligned} \quad (45)$$

where $A(x;k)$, etc. are the Wigner transforms of A , B and C and the differential operators act on A and B separately. The approximate expression in terms of 4-dimensional Poisson bracket $\{A, B\} = \partial_k A \partial_x B - \partial_x A \partial_k B$ defines the first order *gradient expansion*. To this order separating real and imaginary parts one obtains for the Wigner densities $\mp i G^{-+}$ [29]

$$\begin{aligned} &\left\{ S(k) - \Sigma(x, k), iG^{-+} \right\} - \left\{ iG(x, k), \Sigma^{-+}(x, k) \right\} \\ &= \Sigma^{-+}(x, k) G^{+-}(x, k) - \Sigma^{+-}(x, k) G^{-+}(x, k) \\ &\text{with } \Sigma = (\Sigma^R + \Sigma^A)/2, \quad G = (G^R + G^A)/2. \end{aligned} \quad (46)$$

Here $S(k) = \epsilon - \mathbf{k}^2/(2m)$ or $S(k) = k^2 - m^2$ is the Wigner form of the Schrödinger or Klein-Gordon operator (36). The first Poisson bracket on the left side gives the usual Vlasov part. On the right side $\Sigma^{-+} G^{+-}$ and $\Sigma^{+-} G^{-+}$ define gain and loss terms. This transport equation is quite general and as the original Dyson equation still accounts for off-mass-shell processes, part of which are contained in the peculiar second Poisson bracket according to Botermans and Malfliet [29]. We will see that the account of the finite damping width and the inclusion of higher order diagrams for the self energies (sect. 4.5) are essential to extend the scheme beyond classical transport concepts.

Equation (46) by itself is not yet complete, since it requires a relation between G^{-+} and G^{+-} , which normally is provided by a certain physical "ansatz". Under near on-shell conditions, where the Wigner densities are well peaked close to a single on-shell energy $\epsilon \sim \epsilon_{\mathbf{p}}$, c.f. next subsection, one can use the Kadanoff - Baym ansatz or apply the QPA (see Appendix A). Then the integral over ϵ reduces (46) to a familiar form [27,31]

$$\begin{aligned} &\left\{ \partial_t + \mathbf{v} \partial_{\mathbf{x}} - (\partial_{\mathbf{x}} \epsilon_{\mathbf{p}}) \partial_{\mathbf{p}} \right\} n(\mathbf{x}, \mathbf{p}, t) \\ &= \left(\pm i \Sigma^{-+} (1 \mp n(\mathbf{x}, \mathbf{p}, t)) + i \Sigma^{+-} n(\mathbf{x}, \mathbf{p}, t) \right) Z_{\mathbf{p}} \\ &= \left(\pm i \Sigma^{-+} - \Gamma n(\mathbf{x}, \mathbf{p}, t) \right) Z_{\mathbf{p}}, \end{aligned} \quad (47)$$

for the on-shell particle densities of non-rel. fermions or rel. bosons

$$n_F(\mathbf{x}, \mathbf{p}, t) = -i \int \frac{d\epsilon}{2\pi} G_F^{-+}, \quad n_B(\mathbf{x}, \mathbf{p}, t) = i \int \frac{d\epsilon}{2\pi} 2\epsilon G_B^{-+}. \quad (48)$$

Here $\mathbf{v} = \partial_{\mathbf{p}}\epsilon(\mathbf{p})$ is the group velocity, and $Z_{\mathbf{p}} = 1/(1 - \partial\text{Re}\Sigma^R/\partial\epsilon)$ for non-relativistic fermions and $Z_{\mathbf{p}} = 1/(2\epsilon - \partial\text{Re}\Sigma^R/\partial\epsilon)$ for relativistic bosons is a normalization factor. In all expressions ϵ is determined by the dispersion relation $\epsilon = \epsilon(\mathbf{p})$, c.f. (50) below.

The form of the collisional integral in (47) is convenient in many cases, e.g. to extract stationary solution (cf. next subsection) or for the relaxation time approximation, where $1/\Gamma Z_{\mathbf{p}}$ is the corresponding collision time, see (A.4). In the diffusion approximation of eq.(47) one easily recovers eq.(14). The usual Boltzmann-like form of the collisional integral is obtained from the lowest order self energy diagram which in QPA contributes to $\text{Im}\Sigma^R$ (usually second order in the two body interaction), c.f. [27,31] and (66) in sect. 4.8. More general schemes beyond QPA are suggested in sect. 4.7. The photon production rate, eq. (3), is a simple case of (47).

4.4 Stationary and Equilibrium Properties

For a homogeneous stationary system in Wigner ($x; p$) representation all Green's functions become space-time independent and the \odot operation reduces to a simple product for the remaining 4-momentum part in the Dyson equation (37). With $p = (\epsilon, \mathbf{p})$ we therefore drop the x -argument. Eqs. (40) can then be solved algebraically

$$G_F^R(p) = \frac{1}{\epsilon + \mu_F - \epsilon_{\mathbf{p}}^0 - \Sigma^R(p)}, \quad G_B^R(p) = \frac{1}{(\epsilon + \mu_B)^2 - (\epsilon_{\mathbf{p}}^0)^2 - \Sigma^R(p)}, \quad (49)$$

while $G^A(p) = (G^R(p))^*$ and $\Sigma^A(p) = (\Sigma^R(p))^*$. The dispersion relations are

$$\begin{aligned} \epsilon + \mu_F &= \epsilon_{\mathbf{p}}^0 + \Sigma_F^R(\epsilon + \mu_F, \mathbf{p}), & \epsilon_{\mathbf{p}}^0 &= \mathbf{p}^2/2m & \text{(non-rel. fermions)} \\ (\epsilon + \mu_B)^2 &= (\epsilon_{\mathbf{p}}^0)^2 + \Sigma_B^R(\epsilon + \mu_B, \mathbf{p}), & (\epsilon_{\mathbf{p}}^0)^2 &= \mathbf{p}^2 + m^2 & \text{(rel. bosons)} \end{aligned} \quad (50)$$

with corresponding free on-shell energies $\epsilon_{\mathbf{p}}^0$ and chemical potentials μ_B and μ_F . With $\Gamma(p) = -2\text{Im}\Sigma^R(p) = i(\Sigma^{-+}(p) - \Sigma^{+-}(p))$ the spectral function (43) are

$$\begin{aligned} A_F(p) &= \frac{\Gamma(p)}{\left(\epsilon + \mu_F - \epsilon_{\mathbf{p}}^0 - \text{Re}\Sigma^R(p)\right)^2 + (\Gamma(p)/2)^2} & \text{(non-rel. fermions),} \\ A_B(p) &= \frac{\Gamma(p)}{\left((\epsilon + \mu_B)^2 - (\epsilon_{\mathbf{p}}^0)^2 - \text{Re}\Sigma^R(p)\right)^2 + (\Gamma(p)/2)^2} & \text{(rel. bosons).} \end{aligned} \quad (51)$$

They satisfy the sum rules

$$\int_{-\infty}^{\infty} A_B(p) 2\epsilon \frac{d\epsilon}{2\pi} = 1 \quad \text{and} \quad \int_{-\infty}^{\infty} A_F(p) \frac{d\epsilon}{2\pi} = 1. \quad (52)$$

The generalization to relativistic fermions with gamma-matrices up to tensor interactions can be found in ref. [44]. For illustration and later use we give the equilibrium results explicitly, which follow from the stationary condition $\Sigma^{-+}(p)G^{+-}(p) = \Sigma^{+-}(p)G^{-+}(p)$, c.f. eq. (46), and the Kubo-Martin-Schwinger condition [17]

$$\Sigma^{-+}(p) = \Sigma^{+-}(p)e^{-\epsilon/T}. \quad (53)$$

Then all the Green's functions can be expressed through either retarded or advanced Green's functions. From (34), (35) and (41) one then finds

$$\begin{aligned} G^{-+}(p) &= (1 \mp n_\epsilon)G^R(p) \pm n_\epsilon G^A(p), & G^{-+}(p) &= \pm i n_\epsilon A(p), \\ G^{+-}(p) &= -i(1 \mp n_\epsilon)A(p), & G^{++}(p) &= -(1 \mp n_\epsilon)G^A(p) \mp n_\epsilon G^R(p), \end{aligned} \quad (54)$$

and the relations for the four components of the self energies

$$\begin{aligned} \Sigma^{--} &= \Sigma^R \pm i n_\epsilon \Gamma(p), & \Sigma^{-+} &= \mp i n_\epsilon \Gamma(p), \\ \Sigma^{+-} &= i(1 \mp n_\epsilon) \Gamma(p), & \Sigma^{++} &= -(\Sigma^{--})^*, \end{aligned} \quad (55)$$

where the thermal occupations at temperature T (Fermi-Dirac or Bose-Einstein distributions) are

$$n_\epsilon = \{\exp[\epsilon/T] \pm 1\}^{-1}. \quad (56)$$

In the general non-equilibrium case there are no such simple relations between Green's functions and self energies as at equilibrium. In order to proceed one may simplify the problem applying so called Kadanoff-Baym ansatz (given in Appendix A) or using the QPA.

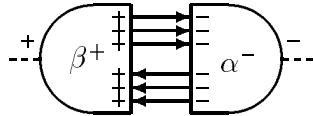
4.5 Diagrammatic Decomposition into Physical Sub-Processes

There have been many attempts in the literature to eliminate the redundancy in the definition of the four Green's function components. We do not like to follow such schemes and rather prefer to keep all four components as they are, since they display a symmetry between the time-ordered and the anti-time ordered parts, i.e. between

the "bra" and "ket" parts of the correlator⁹.

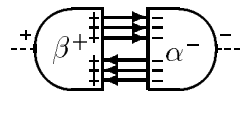
In this formulation physical observables like densities, production rates, etc., are always given by diagrams, where the external vertices appear in conjugate pairs, i.e. with fixed opposite signs, just defining correlation functions. If Fourier transformed over space-time differences they have the properties of Wigner functions. Special examples are the off-diagonal components of the Green's functions and self energies, which define Wigner densities and gain or loss rates, respectively. Working with full Green's functions such correlation diagrams are given by a sum of all topologically distinguished skeleton diagrams with the fixed external vertices of opposite signs. Each diagram of given topology consists of 2^ν terms, where ν is the number of internal vertices, due to the $-+$ summations. These extra summations make this approach rather non-transparent. In this section, however, we like to suggest a very simple classification of correlation diagrams and a reformulation of the corresponding sum, which amends a simple physical interpretation.

We start with the observation, that at least in one way any correlation diagram of given topology and given sign assignments at all vertices can be decomposed into two pieces, such that each of the two sub pieces is a connected diagram which carries only one type of sign on all its external vertices¹⁰



$$(57)$$

The reason for such a decomposition is that then each diagram is given by a "product" of two sub diagrams α^- and β^+ with the same external lines, which one may call amplitude - and adjoint amplitude diagrams. Here α and β denote amplitude diagrams including sign assignments. The adjoint α^+ of any amplitude diagram α^- is given by inverting the senses of all propagator lines and inverting the signs of all vertices; the respective values are conjugate complex to each other $(\alpha^-)^* = \alpha^+$. For amplitude diagrams only the external vertices have definite signs, while internal vertices have still no sign restrictions. In analytical terms the decomposition (57) can be written as



$$(58)$$

$$= (\mp i) G^{-+}(p_1) \dots i G^{+-}(p_m) \beta^+(p_1, \dots, p_m) \alpha^-(p_1, \dots, p_m)$$

$$= (\mp i) G^{-+}(p_1) \dots i G^{+-}(p_m) \left(\beta^-(p_1, \dots, p_m) \right)^* \alpha^-(p_1, \dots, p_m)$$

⁹In thermal field theory the "+" vertices are often considered as ghosts. We do not like to support this viewpoint as these conjugate vertices are as physical as the "-" ones for the full correlation matrix element!

¹⁰For the construction: just deform the diagram such that all + and - vertices are placed left and respectively right from a vertical division line and cut along this line. Pieces which then become disconnected are to be reconnected to the other side until two connected sub-pieces remain. In case that disconnected pieces appear on both sides the result may depend on the order of reconnection and consequently different decompositions are possible.

is void of double counting. It amends a straight forward interpretation in terms of physical scattering processes between certain in – and out-states. These processes occur with partial rates R , which can be positive or negative. The warning to be formulated at this instance is, that if one works with full Green’s functions which also include the finite damping width Γ , particular care has to be taken. The unconsidered account of certain Feynman amplitudes together with finite width spectral functions for the particles, as sometimes done heuristically, may lead to serious inconsistencies.

On the other hand the important point to realize at this level is that the so defined decomposition gives rise to a generalized formulation of transport theories, where multi-particle processes can be considered in a well defined scheme even if one permits for off-shell propagation. Note in particular: for a theory of fermions interacting with bosons the contribution with the fewest number of external particles is just three (rather than four as in the Boltzmann equation). It results from the decomposition a one-loop diagram and allows for one particle *in* and two *out* and vice versa, . Thus, in dense matter an off-shell fermion can just decay into a fermion plus boson or the opposite can happen, e.g. see [31,45]. For these processes it is important that all particles have a finite damping width in dense matter, so that creation and decay modes, which are forbidden from energy-momentum conservation in free space, may occur without principle restrictions in dense matter.

Please note that our decomposition rules are different from the standard cutting rules which only apply either to the set of perturbation theory diagrams [46] or to the set of the quasi-particle diagrams [41]. There diagrams are cut across all $+-$ lines, each cut providing an on-shell delta function from the zero width spectral functions. Diagrams that can be cut into more than two pieces contain a product of more than one delta-function on total energy conservation and therefore show a singular behavior which is not present in the final correlation function. Therefore all such ”multi”-cut diagrams have to cancel out. Such arguments can no longer be given in the case that all spectral functions have finite widths, where the set of diagrams is reduced to the set of skeleton diagrams. Thus, such diagrams have also to be considered in a description with full Green’s functions!

4.6 Three and Four Point Functions

In principle one can stick to the above picture since all infra-red divergences disappear for all diagrams due to the finite propagation times of all Green’s functions. However one may have to consider still quite a numerous amount of diagrams in order to achieve meaningful results. For instance on the QP level we expect, that the proper *in-medium* current appears at both external vertices in a symmetric fashion. Thus for the convective currents one expects

$$j^\nu \simeq ev^\nu = e \frac{\partial}{\partial p_\nu} \epsilon(\mathbf{p}) = e \left(\frac{\partial}{\partial p_\nu} \epsilon_{\mathbf{p}}^0 + \frac{\partial}{\partial p_\nu} \text{Re}\Sigma^R \right) / \left(1 - \frac{\partial}{\partial \epsilon} \text{Re}\Sigma^R \right), \quad (62)$$

where $\epsilon(\mathbf{p}) = \epsilon_{\mathbf{p}}^0 + \text{Re}\Sigma^R(\epsilon(\mathbf{p}), \mathbf{p})$ defines the QP energy momentum relation, see eq. (A.3) in Appendix A. In diagrammatic terms this can be achieved by certain partial resummation that lead to vertex corrections. Thereby we shall not consider an immediate resummation to the exact full vertex, since this would amount to solve the whole problem. Rather we like to stay to a picture where in certain limits like the QPA and QC limit, piece by piece an interpretation in physically meaningful terms can be given.

The considerations in the preceding subsection assigned a particular role to the full $-+$ and $+ -$ Green's functions as Wigner densities. This suggests to apply further resummations and to extend the ideas put forward in ref. [41] in the context of quasi-particles now to particles with finite width. Namely, one likes to gather diagram pieces that are void of the Wigner densities G^{-+} or G^{+-} , both for fermions and bosons. That is, one likes to resum sub-pieces of skeleton diagrams with given number and type of external vertices (3 point or 4 point functions, for example) where all internal and external vertices have only one definite sign value. The $\{-\}$ diagrams then contain only time-ordered full Green's functions G^{--} and therefore represent a straight forward generalization of the standard zero temperature Feynman 3 or 4 point functions now including the full self energies. The $\{+\}$ diagrams are just the adjoined expressions. This way one can define 4 point functions (in-medium interactions)

$$\text{Thick bar} = \text{Diagram 1} + \text{Diagram 2} + \text{Diagram 3} + \dots \quad (63)$$

Here the thick wavy lines relate to the corresponding G_B^{--} -exact boson propagators or two-body potentials in non-relativistic theories with potentials. Since only like sign vertices are permitted, no G^{-+} and G^{+-} lines appear in these functions. Such resummed expressions have been proven useful in the low temperature QPA to define in-medium interactions and effective vertices and they appear also quite meaningful in the limit of low densities, as in the classical limit for example. Various approximation levels are possible for the 4-point functions; a detailed discussion would be beyond the scope of this presentation. We mention just a few possibilities:

- a) a ladder summation in the s -channel (horizontal in diagram (63)) for the particle-particle (p - p) and particle-hole (p - h) channels generalizes the Bruckner G -matrix to non-equilibrium;
- b) in many practical cases (e.g. Landau - Migdal's Fermi-liquid theory [21,22]) the 4-point functions are approximated by 2-point approximants in the t -channel (vertical in (63)). Then RPA-type resummations are possible [41,10], which iterate p - h " $-$ " and " $+$ " loops in the t -channel; details are given in Appendix B; where also the scheme of the bosonization of the interaction is presented, cf. [10,50].
- d) the ultimate could be a crossing and exchange symmetric form; in this case one relies on suitable parameterizations.

These like-sign effective interactions generalize the two-body scattering matrix in

matter to non-equilibrium. Thereby one does not only account for the change of the fermionic occupations (as already considered in the literature) but also includes the damping of the fermions. In this respect it would be interesting to see, how bound states (e.g. the deuteron [51] or the J/Ψ) change their properties in dense matter (Mott transition) also due to the damping widths. For consistency these like-sign effective interactions then also enter the definition of the in-medium vertices (3 point functions) defined as

$$\text{---} \overset{-}{\bullet} \begin{array}{l} \nearrow \\ \searrow \end{array} = \text{---} \begin{array}{l} \nearrow \\ \searrow \end{array} + \text{---} \begin{array}{l} \nearrow \\ \searrow \end{array} \quad (64)$$

4.7 Key diagrams

For simplicity we confine the discussion to the case where the 'external' photon just couples to fermions. Any generalization to other types of particles (external and source internal) is straight forward. Due to the above considerations from now on the remaining diagrams include the following elements: full fermion Green's functions, like-sign 4-point interactions and the corresponding vertices. Please notice that this reduces the set of diagrams even further! In particular not all sign combinations are permitted any longer since some of them are already included in the resummed 3 or 4 point functions.

All photon self-energy diagrams can be build up by iterative four point insertions. Thus, the set of diagrams for Π^{-+} reduces to

$$\begin{array}{l} \text{---} \overset{+}{\circlearrowleft} \text{---} \overset{-}{\Pi} \text{---} = \text{---} \circlearrowleft \text{---} + \text{---} \circlearrowleft \text{---} + \text{---} \circlearrowleft \text{---} + \dots \\ + \text{---} \circlearrowleft \text{---} + \text{---} \circlearrowleft \text{---} + \text{---} \circlearrowleft \text{---} + \dots \end{array} \quad (65)$$

This set of "key"- diagrams is important for all subsequent considerations and therefore deserves further comments.

- (i) Each diagram in (65) represents already a whole class of perturbative diagrams of any order in the interaction strength and in the number of loops. The most essential term is the one-loop diagram¹², which is positive definite, and corresponds to the first term of the classical Langevin result for Π_{cl} in (24) as we shall show later. The other diagrams represent interference terms due to rescattering.

¹²In perturbation theory or QPA the corresponding one-loop diagram usually vanishes for on-shell photons due to conservation laws. Here however, with full Green's and vertex functions it represents a series of perturbative diagrams as the reader can easily imagine.

- (ii) Compared to conventional diagrams, vertex corrections can appear on both sides of one loop as they are separated by $\{+-\}$ lines (see example given in Appendix B).
- (iii) Note that the restriction to like sign vertices for the resummations (64) and (63) are defined with respect to skeleton diagrams in terms of full Green's functions. "Opened" to perturbative diagrams with thin G^0 lines, these can still contain alternative signs, since Dyson's equation (37) includes all signs in the intermediate summations!
- (iv) In some simplified representations (being often used) the 4-point functions behave like intermediate bosons (e.g. phonons), c.f. Appendix B.
- (v) For particle propagation in an external field, e.g. infinitely heavy scattering centers, only the one-loop diagram remains, since the one deals with a genuine one-body problem. However, extra complications arise, since translation invariance is generally broken and the Green's functions then also depend on x .

4.8 Decomposition of Closed Diagrams into Feynman Amplitudes in the QPA

The QPA is quite commonly used concept originally derived for Fermi liquids at low temperatures (Landau-Migdal, see [21,22]). There one deals with on-mass-shell fermions in matter (quasi-particles) described by the pole part of the Green's functions, i.e. one assumes that $\text{Im}\Sigma_F^R \rightarrow 0$ in the Green's function G_F^R . Then with the help of some phenomenologically introduced interaction (particle-hole irreducible) one calculates the values $\text{Re}\Sigma^R$ and $\text{Im}\Sigma^R$ which now depend on quasi-particle properties. Since in QPA the finite width contributions have to appear in higher order through corresponding $\text{Im}\Sigma$ -insertions the whole set of QPA diagrams defining the full $-i\Pi^{-+}$ is by far larger, than set (65).

The QPA has considerable computational advantages as Wigner densities (" $- +$ " and " $+ -$ " lines) become energy δ -functions, and the particle occupations can be considered to depend on momentum only rather than on the energy variable¹³. Formally the energy integrals in eq.(5), (65) can be eliminated, in diagrammatic terms just cutting the corresponding " $- +$ " and " $+ -$ " lines [41]. This way one establishes a correspondence between correlation diagrams (65) and usual Feynman amplitudes in terms of QPA asymptotic states and QPA Green's functions. Thus the QPA allows a transparent interpretation of correlation diagrams.

For the dynamics of the fermion transport the first QPA diagram that contributes to the gain (loss) term

¹³The later approximation is also often used beyond the scope of the QPA and is then known as Kadanoff-Baym ansatz, see [25] and Appendix A, c.f. [12]

$$\begin{aligned}
& - \int \frac{d\epsilon_1}{2\pi} \Sigma^{-+}(p_1) G^{+-}(p_1) \simeq \left\{ \begin{array}{c} \text{+} \\ \text{+} \end{array} \begin{array}{c} \text{+} \\ \text{+} \end{array} \right\}_{\text{QPA}} (1 - n_1) \\
& \longrightarrow \int d^4 p_2 \dots d^4 p_4 \left| \begin{array}{c} \text{+} \\ \text{+} \end{array} \right|^2 \delta^4(p_1 + p_2 - p_3 - p_4) (1 - n_1) (1 - n_2) n_3 n_4
\end{aligned} \tag{66}$$

leads to the standard Boltzmann collision term with corresponding occupation and Pauli suppression factors for the in and out states. Here and below the full blocks denote the effective two-fermion interactions, and thick fermion lines denote the QPA states or Green's functions.

For the here studied photon rates we discuss in detail the correlations diagrams on the right side of (65) with consecutive numbers 1 to 6. Thereby diagrams 1, 2, 4 and 5 describe the bremsstrahlung related to a single in-medium scattering of two fermionic quasi-particles and can be symbolically expressed as Feynman amplitude (67a)

$$\begin{array}{cc}
(a) & (b) \\
(c) & (d)
\end{array} \tag{67}$$

The full circle denotes the effective vertex. One should bear in mind that the photon may couple to any of the external fermion legs and all exchange combinations are possible. The one-loop diagram in (65) is particular, since its QP approximant vanishes for real or time-like photons. However the full one-loop includes QPA graphs of the type (67b), which survive to the same order in $\Gamma/\bar{\epsilon}$ as the other diagrams [41]. In fact it is positive definite and corresponds to the absolute square of the amplitude (67a), c.f. (61). The other diagrams 2, 4 and 5 of (65) describe the interference of amplitude (67a) either with those where the photon couples to another leg or with one of the exchange diagrams. Thereby for neutral interactions diagram (65:2) is more important than diagram 4, while this behavior reverses for charge exchange interactions (the latter is also important for gluon radiation from quarks in QCD transport due to color exchange interactions). Diagrams like 3 describe the interference terms due to further rescatterings of the source fermion with others. According to our rules the diagram (65:3) corresponds to a two-body collision process and describes the interference of amplitude (67c) with that one where the photon couples to the initial leg. Diagram (65:6) describes the photon production from intermediate states and is given by Feynman graph (67d). In the soft photons limit ($\omega_q \ll \epsilon_F$) this diagram (67d) gives a smaller contribution to the photon production rate than the diagram (67a) in QPA, where the normal bremsstrahlung contribution diverges like $1/\omega_q$ compared to the $1/\epsilon_F$ -value typical for the coupling to intermediate fermion lines [47]. However in some specific cases the process (67d) might be very important even in the soft limit. This is indeed the case for so called modified URCA process $nn \rightarrow npe\bar{\nu}$ which is of prime importance in the problem of neutrino radiation from the dense neutron star interior, see [45].

Some of the diagrams, (c.f. the graph shown in footnote 7) which are not presented explicitly in eq.(65) give more than two pieces, if being cut, so they do not reduce to the Feynman amplitudes.

For the validity of the QPA one normally assumes that $\Gamma \ll \bar{\epsilon}$, where $\bar{\epsilon}$ is an average particle kinetic energy ($\sim T$ for equilibrium matter). With $\Gamma \sim \pi^2 T^2 / \epsilon_F$ for Fermi liquids, c.f. (A.5), the QPA constitutes a consistent scheme for all thermal excitations $\Delta\epsilon \sim T \ll \epsilon_F$. However with the application of transport models to higher energies this concept has been taken over to a regime where its validity can no longer easily be justified. Moreover, our considerations show that the condition $\Gamma \ll \bar{\epsilon}$ is not at all sufficient. Rather one has to demand that also $\omega \gg \Gamma$ in the QPA, since finally energy differences of order ω appear¹⁴. In particular, the remaining series of QPA-diagrams is *no longer convergent* unless $\omega > \Gamma$, since arbitrary powers in Γ/ω appear, and there is no hope to ever recover a reliable result by a finite number of QPA-diagrams for the production of soft quanta! With *full Green's functions*, however, one obtains a description that uniformly covers both the soft ($\omega \ll \Gamma$) and the hard ($\omega \gg \Gamma$) regime.

5 The Quasi-classical Limit (QC)

In this section we like to discuss, which class of diagrams remains in the quasi-classical limit and how this is to be interpreted.

The QC limit requires that

- i)* all occupations of the source particles are small ($\langle n_{\mathbf{p}} \rangle \ll 1$) implying a Boltzmann gas with $\mu \ll -T$ and that
- ii)* all inverse length or time-scales times \hbar are small compared to the typical momentum and energy scales of the source systems.

In particular this implies $\hbar\omega, \hbar|\mathbf{q}| \ll \bar{\epsilon}$, and a collision rate $\Gamma = \hbar/\tau_{\text{coll}} \ll \bar{\epsilon}$, where $\bar{\epsilon}$ is a typical particle kinetic energy ($\sim T$ for equilibrium matter). To be precise: ω and \mathbf{q} of the produced particle are sensitive to the space-time structure of the source, while they are negligible as far as energy and momentum balances are concerned. The latter fact permits to prove the Kadanoff–Baym ansatz in this case (see Appendix A and discussion of eq. (84) below) which considers the occupations of the source particles to dependent only on momentum $n_{\mathbf{p}} = n_{\epsilon_{\mathbf{p}} - \mu_F}$ but no longer on energy ϵ . Also we assume that Γ will not depend on time in between subsequent collisions ($|\tau| \sim 1/\Gamma$).

We note in particular that for bosons with chemical potential $\mu_B = 0$, like the produced photon, the *equilibrium* occupations will be large, $n_B \approx T/\omega \gg 1$! This

¹⁴This statement is particular, since one compares the photon energy ω with the damping width of the source particles Γ , while the damping rate of the photon itself $\gamma \simeq |\Pi^{-+}| / (2\omega n_{\omega}^B) < 4\pi e^2 \rho_0 / (\Gamma m) \sim 60 \text{MeV}^2 / \Gamma$ for nuclear matter can be quite small!

fact is of no further relevance, if one excludes internal photon lines in the proper correlation functions (2), Π^{-+} and Π^{+-} as we do.

5.1 Time Structure of Green's Functions and Loops in QC Limit

For fermion Green's functions one has the following simplifications

$$G_F^{-+}(p) \simeq n_{\mathbf{p}}A(p), \quad G_F^{+-}(p) \simeq -i(1 - n_{\mathbf{p}})A(p), \quad (68)$$

while at large temperatures T the particle occupations are given by

$$n_{\mathbf{p}} \simeq \exp[-(\epsilon_{\mathbf{p}} - \mu_F)/T] \ll 1. \quad (69)$$

The correspondence between the diagrammatic expansion (65) and classical limit of sect. 3 becomes more transparent if one uses the mixed $\tau - \mathbf{p}$ representation for the Green's functions, where τ is the time difference between the two space-time points. Then from the definition of G^{-+} and G^{+-} Green's functions (see eq. (34)) one immediately finds for fermions

$$G_F^{-+}(\tau, \mathbf{p}) \simeq n_{\mathbf{p}} \exp[-|\Gamma\tau|/2 - i\epsilon_{\mathbf{p}}\tau], \quad (70)$$

$$G_F^{+-}(\tau, \mathbf{p}) \simeq -i(1 - n_{\mathbf{p}}) \exp[-|\Gamma\tau|/2 - i\epsilon_{\mathbf{p}}\tau], \quad (71)$$

while $G_F^{- -} = (1 - n_{\mathbf{p}})G_F^R - n_{\mathbf{p}}G_F^A$ and $G_F^{++} = -(1 - n_{\mathbf{p}})G_F^A + n_{\mathbf{p}}G_F^R$ are essentially retarded and advanced, respectively.

A further simplification comes from the time behaviour of fermion-loops, c.f (B.7), which mediate classical energy and momentum transfers. The corresponding time scales $1/\epsilon$ or $1/(\mathbf{v}\mathbf{p})$ are very short on the damping scale $1/\Gamma$, so that such loop insertions become instantaneous. This is the reason, why one recovers a Markovian description for the motion of the source in the classical limit. With these simplifications we now calculate the diagrams (65).

5.2 Self Energy Diagrams in the QC Approximation

In the mixed $\tau - \mathbf{q}$ representation the one loop diagram is given by

$$\begin{aligned} -i\Pi_0^{-+}(\tau, \mathbf{q}) &= \int \frac{d^3p_1 d^3p_2}{(2\pi)^6} V^\mu V^\nu G^{-+}(\tau, \mathbf{p}_1) G^{+-}(\tau, \mathbf{p}_2) (2\pi)^3 \delta(\mathbf{p}_2 - \mathbf{q} - \mathbf{p}_1) \\ &\simeq \int \frac{d^3p}{(2\pi)^3} V^\mu V^\nu n(\mathbf{p} + \mathbf{q}/2) (1 - n(\mathbf{p} - \mathbf{q}/2)) e^{-|\Gamma\tau|} e^{-i(\mathbf{q}\mathbf{v})\tau}, \quad (72) \end{aligned}$$

if $|\mathbf{qv}| \ll T$. Here $V^\mu \approx \sqrt{4\pi}j^\mu(\mathbf{p})$ defines the in-medium photon - fermion vertex in the classical limit following eq. (62), while $\mathbf{p} \approx (\mathbf{p}_1 + \mathbf{p}_2)/2$. Apart from the \mathbf{q} -dependent oscillations the time structure of this diagram is given by an exponential decay: $e^{-|\Gamma\tau|}$ which leads to

$$\begin{aligned} -i\Pi_0^{-+}(\omega, \mathbf{q}) &= 4\pi e^2 \int \frac{d^3p}{(2\pi)^3} n(\mathbf{p} + \mathbf{q}/2)(1 - n(\mathbf{p} - \mathbf{q}/2)) \frac{2\Gamma v^i v^k}{(\omega - \mathbf{qv})^2 + \Gamma^2} \\ &\approx 4\pi e^2 \rho_0 \left\langle \frac{2\Gamma v^i v^k}{(\omega - \mathbf{qv})^2 + \Gamma^2} \right\rangle. \end{aligned} \quad (73)$$

for the spatial components of Π^{-+} . This expression is identical to the $n = 0$ term of the classical Langevin result (25).

The classical Langevin example (sect. 3) considers the propagation of a single charge (say a proton) in neutral matter (e.g neutrons). Therefore for this case only diagrams occur, where both photon vertices attach to the same proton line. Also, of course, no direct proton-proton interactions occur. In the following we like to show that diagrams of the type

$$-i\Pi_{\text{cl}}^{-+} = \text{---}^+ \text{---}^- + \text{---}^+ \text{---}^- + \text{---}^+ \text{---}^- + \dots \quad (74)$$

with $n \{-+\}$ scattering interactions (intermediate particle-hole $\{-+\}$ neutron loops) correspond to the n -th term in the Langevin result (24). To demonstrate this we look into the time structure of such a diagram, and assign times 0 and τ to the external $-$ and $+$ vertices, while the $-$ and $+$ interactions are taken at t_1^- to t_n^- and t_1^+ to t_n^+ , respectively. In the classical limit G^{--} is retarded, while G^{++} is advanced (see eqs. (35), (70) and (71)), such that both time sequences have the same time ordering: $0 < t_1^- < \dots < t_n^- < \tau$ and $0 < t_1^+ < \dots < t_n^+ < \tau$ (all inequalities reverse, if all line senses are reversed). Thus the τ -dependence of the modulus of these diagrams gives $e^{-|\Gamma\tau|}$. A second simplification emerges from the fact that the $+-$ loop interaction insertions mediate classical momentum transfers $|\mathbf{p}_n - \mathbf{p}_{n+1}|$ which are large compared to $\hbar\Gamma$. Therefore the time structure of these loops becomes very short on the scale $1/\Gamma$ and therefore merge $\delta(t_n^- - t_n^+)$. With $t_n = t_n^- = t_n^+$ diagram (74) then no longer depends on the intermediate times t_n apart from the ordering condition, and therefore results in a factor $|\Gamma\tau|^n/n!$. With $\hbar\mathbf{q} = 0$ also the corresponding momenta are pair-wise identical, and the remaining momentum integrations just serve to define the correlation between \mathbf{v}_m and \mathbf{v}_{m+n} after n scattering. Thus

$$\begin{aligned} \text{---}^+ \text{---}^- &= \text{---}^+ \text{---}^- + \text{---}^+ \text{---}^- + \text{---}^+ \text{---}^- + \dots \quad (75) \\ &= \begin{cases} -i\Pi_n^{-+}(\tau, \mathbf{q} = 0) \simeq 4\pi e^2 \rho_0 \langle v_m^i v_{m+n}^k \rangle_m \frac{|\Gamma\tau|^n}{n!} e^{-|\Gamma\tau|} \\ -i\Pi_n^{-+}(\omega, \mathbf{q} = 0) \simeq 4\pi e^2 \rho_0 \langle v_m^i v_{m+n}^k \rangle_m 2\Gamma^n \text{Re} \frac{1}{(\Gamma - i\omega)^{n+1}} \end{cases}, \end{aligned}$$

where the resulting proportionality to the proton density ρ_0 results from $-+$ and $+-$ Green's functions next to the external vertices. Here of course we have silently assumed a consistency condition to be fulfilled: namely that the interaction loops which one takes into account also consistently define the damping width Γ of the source particles! In particular the extra powers in occupations coming from the $+-$ loops are contained in Γ , and therefore do no longer explicitly appear in the final result. This proves that in the classical limit these diagrams reproduce the terms of the classical Langevin series (24).

5.3 Hierarchy of the QC expansion

The Langevin diagrams (75) have the following properties:

- a) *external vertices*: the external photon couples to the same fermion line;
- b) *topology*: the diagrams are planar, i.e. no crossing of lines occur.
- c) *$-+$ sign topology*: if one cuts them at all $-+$ lines they decompose precisely into two pieces;
- d) *value*: apart from the velocity correlations they all give the same contribution to the soft photon point $(\omega, \mathbf{q}) = 0$;

Using the equal time properties of classical $-+$ -loop interaction insertions one finds that

$$\begin{array}{c} + \\ \oplus \\ \ominus \\ - \end{array} \begin{array}{c} + \\ \oplus \\ \ominus \\ - \end{array} = \int_0^\infty \Gamma e^{-\Gamma\tau} d\tau = 1, \quad \text{while} \quad \begin{array}{c} + \\ \oplus \\ \ominus \\ - \end{array} \begin{array}{c} + \\ \oplus \\ \ominus \\ + \end{array} = \int_0^\infty n\Gamma e^{-\Gamma\tau} d\tau = n \quad (76)$$

at $\mathbf{q} = 0$, where n is the proton occupation. The left case iteratively enters the Langevin diagrams and one compiles factors of unity for each time folding, since the loop insertions of order Γ are compensated by the time integration over the Green's function product $G^{--}G^{++}$. This proves d).

What remains to be shown is that for the classical problems discussed in sect. 3 all other key diagrams are disfavored by extra occupation factors n or $\Gamma/\bar{\epsilon}$ which both are small compared to unity.

To a): Since in the classical problems of sect. 3 only a single charged particle (say a proton) in neutral matter is considered, all diagrams with more than one proton line do not occur in this case. To b): Non-planar diagrams, where interactions cross, violate classical time-ordering. Either the two interaction times are interlocked on a time scale $1/\bar{\epsilon}$ and therefore lead to a penalty factor $\Gamma/\bar{\epsilon}$ or restoring the time-ordering one obtains a Z-shape fermion line, which gives an extra occupation factor n . To c): Diagrams that can be cut into more than two pieces can be obtained on various ways: i) by any $-+$ -loop insertion which switches signs on the outer proton lines, thus using the right insertion in (76); here one obtains an extra hindrance factor n . ii) extra insertions of $--$ or $++$ blocks linking the outer proton lines;

since there are no direct proton-proton interactions these effective interactions are mediated by the surrounding neutron matter thus containing $--$ neutron loops, which also leads to an additional factor n , besides another n factor due to the $-+$ proton Green's function.

6 General Quantum Consideration for Hot and Dense Matter

The considerations above show the following. A proper treatment of an entirely classical problem, namely the coupling of a classical source to a wave (electromagnetic field), on the level of quantum many-body theory requires technics, that even nowadays are still non-standard, i.e. beyond perturbation theory or QPA. While the classical problem can be solved quite conveniently and simple with no problems on the infra red side, the corresponding quantum description requires an appropriate account of the finite damping width Γ of the source particles. The most natural approach in our mind is the real-time Green's function technic, which however requires partial resummation, such that the finite width is included already on the one-body Green's function level.

In this section we analyze the production rate from hot and dense matter in the quantum case in terms of non-equilibrium Green's functions. In order to provide some analytical results which easily can be discussed in different limiting cases, we employ the following approximation for the full retarded Green's function. We assume G^R to be given by a simple pole approximation with constant residue

$$G_R^F = \frac{1}{\epsilon + \mu_F - \epsilon(\mathbf{p}) + i\Gamma/2} \quad (77)$$

where $\epsilon(\mathbf{p}) = \mathbf{p}^2/(2m_F^*)$, m_F^* being an effective fermion mass. The width Γ is assumed to be independent of ϵ and \mathbf{p} . Explicit results will be given for the one - and three loop case (the first two diagrams in (65)).

6.1 Qualitative expectations

Compared to the classical results we expect the following changes:

- a) one loses the classical hierarchy of diagrams, such that many more diagrams contribute in the quantum case; for specific couplings, however, some diagrams are disfavored or drop due to selection or suppression rules, e.g. non-planar diagrams in $SU(n)$ coupling;
- b) the radiated quantum carries finite momentum and energy (which vanish in the classical limit), such that additional recoil corrections and phase-space factors $\sim e^{-\omega/T}$ appear; the latter is important, since it cures the classical ultra violet

catastrophe, where the intensity spectrum is white, leading to a divergence of the radiated energy in the classical case;

- c) the occupations are no longer of Boltzmann type with $n \ll 1$, so that Pauli suppression and Bose-Einstein enhancement effects are significant;
- d) the duration time of binary collisions $\sim 1/\epsilon_F$ mediated by interaction loop insertions (B.7) in the correlation diagrams, are no longer negligible compare to $1/\Gamma$ as in the classical case, so that non-markovian memory effects become important [48,49].

Points (b) and (c) can be clarified using the exact relation between thermal fermion and boson occupations

$$n^F(\epsilon + \omega/2)(1 - n^F(\epsilon - \omega/2)) = (n^F(\epsilon - \omega/2) - n^F(\epsilon + \omega/2))n^B(\omega) \quad (78)$$

which simplifies in the following limits to

$$\begin{aligned} n^F(\epsilon + \omega/2)(1 - n^F(\epsilon - \omega/2)) &\approx -\frac{d}{d\epsilon}n^F(\epsilon)n^B(\omega)\omega \quad \text{for } \omega \ll T \\ &\approx n^F(\epsilon)n^B(\omega)\omega/T \quad \text{for } \omega \ll T, n^F \ll 1. \end{aligned} \quad (79)$$

At low temperatures only states close to the Fermi-surface contribute. The last approximate relation suggests that relative to the classical results of sect. 3 an additional phase-space suppression factor $n^B(\omega)\omega/T$ appears in the quantum case, which accounts for the finite energy ω carried away by the quantum.

6.2 Contribution of One-Loop Diagram with Full Fermion Propagators

We first consider the one-loop diagram of (65) with the full fermion propagators

$$\text{---}\overset{+}{\bullet}\text{---}\text{---}\text{---}\overset{-}{\bullet}\text{---} = -i\Pi_0^{-+} = -iV^\mu V^\nu \mathcal{A}_0^{-+} \quad (80)$$

where \mathcal{A}_0^{-+} denotes the bare loop without vertices. For simplicity we will neglect vertex corrections. The later can be trivially included in Landau-Migdal approximation (e.g. see eq. (72), Appendix B and refs. [10,50]).

With the help of relation (78) and the equilibrium form of the Green's functions (54) the bare loop reads

$$-i\mathcal{A}_0^{-+} = n_\omega^B \int \frac{d\epsilon d^3p}{(2\pi)^4} \frac{\Gamma}{(\epsilon + \mu_F - \epsilon_p)^2 + (\Gamma/2)^2} \frac{\Gamma (n_\epsilon^F - n_{\epsilon+\omega}^F)}{(\epsilon + \mu_F - \epsilon_{\mathbf{p}+\mathbf{k}} + \omega)^2 + (\Gamma/2)^2}. \quad (81)$$

This expression can be evaluated in closed form in different limits. We first analyze the QPA (i.e. $\Gamma \ll \omega, kv_F, T$ in case $T \ll \epsilon_F$ or $\Gamma \ll \omega, kv_T \sim k\sqrt{T/m_F^*}$, for

$T \gg \epsilon_F$), which can be found in the literature. In this limit one recognizes two energy δ -functions in eq. (81) (see approximation formula (A.2) of Appendix A), which together with momentum conservation and exact relativistic kinematic can only be fulfilled for space-like (ω, \mathbf{k}) . Following ref. [10] one obtains for the QPA loop in various limits

$$\begin{aligned}
-i\mathcal{A}_0^{-+}(\omega, \mathbf{k})\Big|_{\text{QPA}} &= \begin{cases} 0 & \text{for } \omega \geq |\mathbf{k}| \\ \frac{(m_F^*)^2 T}{2\pi k} n_\omega^B \ln \frac{\exp(\kappa) + 1}{\exp(\kappa) + \exp(-\omega/T)} & \text{for } \omega \ll |\mathbf{k}|, \end{cases} \\
\rightarrow \begin{cases} \frac{(m_F^*)^2 T}{2\pi k} n_\omega^B & \text{for } \kappa \ll -1, \quad \omega \ll |\mathbf{k}| \\ \frac{(m_F^*)^2 T}{2\pi k} \exp(-\kappa) \exp(-\omega/T) & \text{for } \kappa \gg 1, \quad \omega \ll |\mathbf{k}|, \end{cases} \quad (82)
\end{aligned}$$

$$\text{where } \kappa = (m_F^* v^2 / 2 - \mu_F) / T, \quad \text{with } v = (\omega - k^2 / (2m_F^*)) / |\mathbf{k}|.$$

Here non-relativistic kinematics¹⁵ has been used, where v is the recoil corrected fermion velocity that essentially contributes to the loop and the condition $\omega \ll |\mathbf{k}|$ assures $|v| \ll 1$. The simplified expression for $\kappa \ll -1$, realized for $T \ll \epsilon_F \approx \mu_F$ and $\omega < kv_F$, is quite frequently used for space-like interaction loops in low temperature Fermi systems as in Landau's Fermi liquid theory. However, it shows a singular behavior $\propto 1/(k\omega)$ in the small $\omega \ll k = |\mathbf{k}| \ll T$ limit, which is a generic defect of the QPA. The Boltzmann limit $\mu_F \ll -T$ leads to the $\kappa \gg 1$ case, which apart from recoil correction and the extra quantum phase-space factor $e^{-\hbar\omega/T}$ coincides with that for classical diffusion result (20) in sect. 3. In summary, for the one loop term the QPA leads to meaningful results only for large space-like ω, \mathbf{q} (hard thermal loops).

In the general case only the integral in eq. (81) over the angle $\hat{p}\hat{k}$ can be performed

$$\begin{aligned}
-i\mathcal{A}_0^{-+} &= n_\omega^B \int_{-\infty}^{\infty} d\epsilon \int_0^{\infty} \frac{pdpm_F^*}{(2\pi)^3 k} \frac{\Gamma}{(\epsilon + \mu_F - \epsilon_p)^2 + (\Gamma/2)^2} (n_\epsilon^F - n_{\epsilon+\omega}^F) \\
&\times \left[\arctan \frac{\epsilon + \mu_F + \omega - \epsilon_p - \epsilon_k + pk/m_F^*}{(\Gamma/2)} \right. \\
&\left. - \arctan \frac{\epsilon + \mu_F + \omega - \epsilon_p - \epsilon_k - pk/m_F^*}{(\Gamma/2)} \right] \quad (83)
\end{aligned}$$

in closed form. To proceed further we consider the case of small spatial momenta $k = |\mathbf{k}|$ such that $pk \ll m_F^* \Gamma$. For the remaining two-dimensional integral

¹⁵ As a defect of the non-relativistic approximation the result does not exactly vanish for $\omega \geq |\mathbf{k}|$ but rather leads to terms of the order $\exp(-m_F^*/T)$ or less.

$$\begin{aligned}
-i\mathcal{A}_0^{-+} &= \frac{(2m_F^*)^{3/2}}{(2\pi)^3} n_\omega^B \int_{-\infty}^{\infty} d\epsilon (n_\epsilon^F - n_{\epsilon+\omega}^F) \int_0^{\infty} d\epsilon_p (\epsilon_p)^{1/2} \frac{\Gamma}{(\epsilon + \mu_F - \epsilon_p)^2 + (\Gamma/2)^2} \\
&\quad \times \frac{\Gamma}{(\epsilon + \mu_F - \epsilon_p - \epsilon_k + \omega)^2 + (\Gamma/2)^2} \quad \text{for } pk \ll m_F^* \Gamma \quad (84)
\end{aligned}$$

one realizes that the ϵ_p -integration over the product of Lorentz functions gives

$$\frac{4\pi\Gamma\sqrt{\epsilon + \mu_F}}{(\omega - k^2/(2m_F^*))^2 + \Gamma^2} \quad \text{for } \epsilon + \mu_F \gg \Gamma \quad (85)$$

while it is essentially zero for $\epsilon + \mu_F \ll -\Gamma$. For correspondingly small values of Γ one therefore obtains

$$-i\mathcal{A}_0^{-+} \simeq n_\omega^B \frac{\Gamma(2m_F^*)^{3/2}}{2\pi^2[(\omega - k^2/2m_F^*)^2 + \Gamma^2]} \int_0^{\infty} \epsilon_p^{1/2} d\epsilon_p (n_{\epsilon_p - \mu_F}^F - n_{\epsilon_p + \omega - \mu_F}^F), \quad (86)$$

where we have replaced the remaining ϵ variable by ϵ_p . The very same form emerges, if one formally replaces

$$n_\epsilon^F - n_{\epsilon+\omega}^F \rightarrow n_{\epsilon_p - \mu_F}^F - n_{\epsilon_p + \omega - \mu_F}^F \quad (87)$$

in (84) and first integrates over ϵ . This approximation (87) corresponds to the Kadanoff–Baym ansatz (see Appendix A).

Equation (86) valid for $pk \ll m_F^* \Gamma$ can be evaluated in two limits

$$-i\mathcal{A}_0^{-+} \longrightarrow \frac{\omega}{T} n_\omega^B \frac{\Gamma}{(\omega - k^2/(2m_F^*))^2 + \Gamma^2} \begin{cases} m_F^* p_F T / \pi^2 & \text{for } \Gamma, T \ll \epsilon_F \approx \mu_F \\ \rho_F & \text{for } T \gg \epsilon_F, \omega, \Gamma \end{cases} \quad (88)$$

where essential contributions arise from momenta $\sim p_F$ for $T \ll \epsilon_F$ or around $p_T \sim \sqrt{m_F^* T}$ for $T > \epsilon_F$. Here ρ_F is the density of the charged fermions. Compared to the QPA which is zero for time-like momenta, this result is finite and of order $1/\Gamma$ in the soft limit. It agrees with the classical result (25) and the corresponding QC limit (73) besides recoil and the quantum phase-space corrections.

Starting from the QPA for the fermion Green's functions one usually attempts to restore a dependence on the non-zero fermion width for the boson self-energy Σ_B^R by means of the analytical continuation $\omega \rightarrow \omega + i\Gamma$, where

$$\mathcal{A}_0^R = \int \frac{d^3p}{(2\pi)^3} \frac{n_p - n_{\mathbf{p}+\mathbf{k}}}{\epsilon_p - \epsilon_{\mathbf{p}+\mathbf{k}} + \omega + i\Gamma}. \quad (89)$$

In refs. [52,10,53] such a procedure has been used in order to account for the finite Δ -isobar width in the pion self energy. We see that the value $\text{Im}\mathcal{A}_0^R$ given by eq. (89)

and that given by (86) coincide only if $n_{\mathbf{p}+\mathbf{k}} \simeq n_{\epsilon_{\mathbf{p}+\omega}-\mu_F}$, i.e. applying Kadanoff–Baym ansatz.

The thus discussed one-loop diagram can also be used for the intermediate t -channel interaction loops \mathcal{G}^{-+} occurring in higher order diagrams. There the typical values of parameters are

$$\omega < \epsilon_F, \quad k \geq p_F, \quad p \geq p_F. \quad (90)$$

Therefore at least for $\Gamma \ll \epsilon_F$ one has large space-like momenta with $pk \gg \Gamma m_F^*$. Then from eq. (83) one obtains

$$-i\mathcal{A}_0^{-+} = - \int_{-\infty}^{\infty} \frac{(m_F^*)^2}{4\pi^2 k} (n_{\epsilon}^F - n_{\epsilon+\omega}^F) d\epsilon \left[\frac{\pi}{2} + \arctan\left(\frac{\epsilon + \mu_F}{\Gamma}\right) \right], \quad (91)$$

which merges the QPA expressions in (82) for large space-like momenta in the limit $\Gamma \ll \epsilon_F$ both at low temperatures $T \ll \epsilon_F \approx \mu_F$ ($\kappa \ll -1$) and in the Boltzmann limit ($\kappa \gg 1$).

Thus, for the intermediate t -channel interaction loops \mathcal{G}^{-+} one can safely use the QPA ($\Gamma \rightarrow 0$), which even accounts for higher order correction to this loop, as one sees from the corresponding limit of the diffusion result (20). Only for soft loops (e.g. as in the s -channel) the QPA is ill defined.

Comparing the one-loop result at non-zero Γ (88) with the first non-zero diagram in the QPA ($\Gamma = 0$ in the fermion Green's functions)

$$\text{---} \bullet \text{---} \left(\text{---} \bullet \text{---} \right) = C_0(\omega) \left\{ \text{---} \bullet \text{---} \right\}_{\text{QPA}} \quad (92)$$

at small momentum \mathbf{k} one determines a correction factor

$$C_0(\omega) = \frac{\omega^2}{\omega^2 + \Gamma^2}, \quad (93)$$

which cures the defect of the QPA for soft ω . This factor complies with the replacement $\omega \rightarrow \omega + i\Gamma$. A similar factor has been observed in the diffusion result, where however the macroscopic relaxation rate Γ_x enters, due to the resummation of all rescattering processes. Other factors between eq. (88) and in the corresponding QPA Feynman diagram (c.f. ref. [47]) become identical, if one explicitly calculates the width Γ to that order, see also [52].

6.3 Higher Order Diagrams with Full Fermion Propagators

Along similar routes (details are given in Appendix C) the correction factors for the higher order diagrams can be derived. Here we just quote the results for the next lowest order diagrams

$$\text{---} \begin{array}{c} \oplus \\ \circ \\ \ominus \end{array} \text{---} = C_1(\omega) \left\{ \text{---} \begin{array}{c} \oplus \\ \circ \\ \ominus \end{array} \text{---} \right\}_{\text{QPA}} \quad (94)$$

$$\text{---} \begin{array}{c} \oplus \\ \text{---} \\ \ominus \end{array} \text{---} = C_0(\omega) \left\{ \text{---} \begin{array}{c} \oplus \\ \text{---} \\ \ominus \end{array} \text{---} \right\}_{\text{QPA}} \quad (95)$$

with $C_0(\omega)$ from (93) and

$$C_1(\omega) = \omega^2 \frac{\omega^2 - \Gamma^2}{(\omega^2 + \Gamma^2)^2}. \quad (96)$$

The total radiation rate is obtained from all diagrams in (65).

The set of QPA diagrams in (92), (94) and (95) are just those that determine the IQF scattering rate (28) including the exchange diagram for a source of fermions (95). The latter drops in the classical limit, where the two other ones yield the $n = 0$ and $n = 1$ terms of the classical Langevin result (24). Thereby the damping correction factors C_0 and C_1 in the quantum case are the same as classically derived. For $\Gamma \ll \omega$ they tend to unity and the production rate coincides with the QPA results as obtained in ref. [47], while there is a substantial suppression at small frequencies $\omega \ll \Gamma$.

In the corresponding QC limit all the diagrams of type (74) with an arbitrary number of $-+NN$ -interaction insertions can be summed up leading to the diffusion result (18) in sect. 3.1. For small momenta \mathbf{q} this leads to a suppression factor of the form $C = \omega^2/(\omega^2 + \Gamma_x^2)$.

There is hope that even in the quantum case some higher order diagrams can also be resummed and that qualitatively a similar suppression factor emerges like for the diffusion result.

7 Discussion and Perspectives

We investigated the production of particles from the collision dynamics of dense matter at the example of photon production. Thereby the source of charged particles was described in two ways, a) as a classical system governed by classical transport

equations and b) as a quantum system in terms of a real-time non-equilibrium field theory formulation. The central quantity is the current-current correlation function which relates to the imaginary part of the proper self energy of the produced particle. Under quite general assumptions this correlation function governs the local production and absorption rates in the matter. Since the here discussed features are of kinematical origin, relating space-time scales to the corresponding momentum and energy scales, all conclusions drawn in this study are general and therefore also apply to the in-medium production and absorption rates of any kind of particle.

The problem could be quite naturally formulated and solved in the classical descriptions by means of a macroscopic transport and a microscopic Langevin process. These studies showed that spectrum of produced particles is essentially governed by one macroscopic scale, the relaxation rate Γ_x of the source. For frequencies ω of the produced quantum which are large compared to Γ_x the spectrum can be described by the incoherent quasi-free scattering approximation (IQF) used in most of the transport models. Higher order corrections help to improve the result. Once, however, $\omega < \Gamma_x$ this quantum is "soft". It can no longer resolve the individual collisions in time and therefore the IQF picture fails and produces a false infra-red divergence in the rate. Rather, the correct rate is regular and differs from the IQF result by a suppression factor

$$C_0(\omega) = \frac{\omega^2}{\omega^2 + \Gamma_x^2}. \quad (97)$$

This soft part of the spectrum is genuine non-perturbative. The essential features are summarized in figs. 1 and 2 of sect. 3. For relativistic sources a second scale comes in, once the wave number $|\mathbf{q}|$ of the produced particle exceeds the value of $\Gamma_x/\sqrt{\langle v^2 \rangle}$ due to the increased spatial resolution as shown by the closed form results of the diffusion model.

On the quantum level new scales come in since now ω and \mathbf{q} also correspond to the energy and momentum of the photon which have to be compared with the characteristic energy and momentum scales of the source as given by temperature T and chemical potential μ or the Fermi energy ϵ_F . Also the occupations can become degenerate and Pauli suppression or Bose enhancement effects are important. For the general formulation one has to leave theoretical schemes that are based on the concept of asymptotic states like perturbation theory or quasi-particle approximation. The proper frame is the real-time non-equilibrium field theory, where the proper self-energy can be formulated in terms of closed correlation diagrams with general propagators. Thereby the resummation of Dyson's equation to full propagators which also include the imaginary parts of the self energy and therefore account for the damping of the source particles is the essential step to cure the infra-red problem. Only this way one comes to a convergent scheme. After this resummation the corresponding set of diagrams is then reduced to diagrams with skeleton topology. Using the Keldysh $-+$ notations we have addressed a particular role to all $-+$ and $+-$ lines as 8-dimensional Wigner densities of occupied and available

”states”. This motivated further resummations which define in-medium interactions and vertex corrections. The resulting set of diagrams can then be discussed in detail in these physical terms. A decomposition of these correlation diagrams in terms of the interference of two ”amplitude” diagrams is suggested, where Wigner densities enter as in- and out-states. This permits a transparent physical interpretation of the correlations diagrams, which may be used to formulate multi-particle collision processes in matter. They can serve as input for a generalized transport description, which ultimately includes the off-shell propagation of particles and therefore unifies resonances which have a width already in vacuum with all other particles in the dense matter, which acquire a damping width due to collisions.

Once one has the full propagators and the in-medium interactions it is in principle straight forward calculate the diagrams. However both, the computational effort to calculate a single diagram and the number of diagrams, are increasing dramatically with the loop order, such that in practice only lowest order loop diagrams can be considered in the full quantum case. In certain limits some diagrams drop out. In particular we could show, that in the classical limit of the quantum description only a special set of diagrams survive, which could be associated with the multiple collision terms of the classical random Langevin process. Comparing the lowest order loop diagrams in various limits to the corresponding QPA diagrams one realizes that also here correction factors similar to (97) appear. Now the characteristic scale is the damping width Γ of the source particles. Accounting for higher order diagrams one concludes that also in the quantum case the relaxation rate Γ_x is the relevant scale which decides between soft and hard photons. Thus for applications one has to compare the typical energies of the produced particles with the typical relaxation rates of the source system.

Our considerations are of particular importance for the theoretical description of nucleus-nucleus collisions at intermediate to relativistic energies. With temperatures T in the range of 30 to 100 MeV for dense nuclear matter, up to 200 MeV for hadronic matter and beyond 150 MeV for the quark gluon plasma or parton phase most of the kinetic models that are used infer collision rates Γ for the constituents, which during the high density phase can reach the system’s temperature, $\Gamma \lesssim T$. Such estimates make the use of on-shell concepts already rather questionable. The particles uncertainty in energy is comparable with the mean kinetic energy! In particular the bulk production and absorption rates of all particles with masses less than T , if calculated in standard IQF approximation, are seriously subjected to the here discussed effect. Therefore the corresponding quenching factors (97) should sensitively affect the production rates of quark pairs and gluons during the plasma phase, of low energy pions during hadronization and real and virtual photons with correspondingly low energies. Since our discussion was restricted to the production in dense matter, for the particular case of photon production in nuclear collisions one has to consider in addition the radiation caused by the incoming charged ions and outgoing charged fragments. Due to Low’s theorem [57] the latter give rise to an infra-red divergent $\sim 1/\omega$ component which interferes with the one discussed here.

In astrophysics neutrinos produced from neutron stars or during super nova collapse have an absorption mean free path which is long compared to the size of the radiating system (see [7,8,10,54,55]). Thus the production rates cannot be estimated by black-body radiation. Rather the microscopic rates are relevant. The mean kinetic energies per neutrino or $\nu\bar{\nu}$ -pair are about $\sim 3T$ or $\sim 6T$, respectively. With mean collision rates of the order of $\Gamma \sim \pi^2 T^2 / \epsilon_F \ll T$ [56], c.f. eq. (A.5), the production rates can safely be estimated in IQF-approximation for relatively cold neutron stars $T \leq 1.5$ to 2 MeV. Already around $T \sim 5$ MeV the quenching factor (97) is significant (0.3) and it may become even smaller during super nova collapse. Then the temperatures can raise to $T \sim 10 - 30$ MeV such that $\Gamma \sim T$ and the here discussed suppression effects are relevant for the corresponding neutrino emissivity.

Appendix

A Kadanoff–Baym Ansatz and QPA

In the general non-equilibrium case one has no simple relations between Green's functions as in equilibrium. In order to proceed nevertheless one often uses the so called Kadanoff–Baym ansatz [25]. For Fermions it reads

$$G_F^{+-} = 2i(1 - n_{\epsilon_{\mathbf{p}} - \mu_F}^F) \text{Im}G_F^R, \quad G_F^{-+} = -2in_{\epsilon_{\mathbf{p}} - \mu_F}^F \text{Im}G_F^R, \quad (\text{A.1})$$

where $n_{\epsilon_{\mathbf{p}} - \mu_F}^F$ are the fermion occupations which now depend on \mathbf{p} through the on-shell dispersion relation (50) rather than on ϵ . One should note that the Kadanoff–Baym ansatz does not directly follow from the properties of the G^{-+} and G^{+-} functions, rather it has been introduced in order to recover the Boltzmann limit. The correctness of this ansatz has only been proven in the QPA, see [12]. Eqs. (A.1) complies with the definition of the particle densities (48), as can be seen by the sum rules (52).

Dealing with dressed particles we consider only diagrams with thick fermion lines determined from the corresponding Dyson equations. Approximation (A.1) is however based on the assumption that $\text{Im}\Sigma_F^R$ is much smaller than all other energies scales entering the problem.

In particular in the limit $\text{Im}\Sigma_F^R \rightarrow 0$ in the fermion Green's functions one comes to the QPA, where the imaginary part of retarded Green's function becomes a delta function. E.g. for non-relativistic fermions

$$\text{Im}G_F^R \simeq -\pi\delta[\epsilon + \mu_F - \epsilon_{\mathbf{p}}^0 - \text{Re}\Sigma_F^R(\epsilon + \mu_F, \mathbf{p})], \quad (\text{A.2})$$

where the dispersion relation between ϵ and \mathbf{p} is implicitly given by

$$\epsilon_{\mathbf{p}} \simeq \epsilon_{\mathbf{p}}^0 + \text{Re}\Sigma_F^R(\epsilon_{\mathbf{p}}, \mathbf{p}). \quad (\text{A.3})$$

The simple form (A.2) has problems with the sum rule (52), if retardation effects are important ($\partial \text{Re}\Sigma^R/\partial\epsilon \neq 0$), which also contribute to the off-shell part of G_F^R , c.f. ref. [31]. For simplicity we ignore this and also employ a quadratic p -dependence for $\text{Re}\Sigma^R$ in terms of an effective fermion mass $\epsilon_{\mathbf{p}} \simeq \mathbf{p}^2/2m_F^*$ in the applications.

From the dispersion equations one easily finds the corresponding relaxation times. E.g., for fermions supposing that $\text{Im}\Sigma^R$ is small and introducing $\tau_{\text{col}} = 1/2\delta\epsilon$, where we use that $\psi_F \sim \exp(-i(\epsilon_{\mathbf{p}} - i\delta\epsilon)t)$, one finds

$$\tau_{\text{col}} = \left| \left(1 - \frac{\partial \text{Re}\Sigma_F^R}{\partial\epsilon} \right) / \left(2\text{Im}\Sigma_F^R \right) \right|_{\epsilon=\epsilon_{\mathbf{p}}} . \quad (\text{A.4})$$

This value would tend to infinity for $\text{Im}\Sigma_F^R \rightarrow 0$. In reality the fermion width determined by the value $\text{Im}\Sigma_F^R$ is rather large even at sufficiently small temperatures. E.g. for nucleons, applying the QPA for the intermediate nucleon lines, it can be estimated as follows [56]

$$\text{Im}\Sigma_F^R \simeq -|\tilde{M}_F|^2[(1 - \epsilon_{\mathbf{p}}/\epsilon_F)^2 + T^2\pi^2/\epsilon_F^2], \quad T \ll \epsilon_F \quad (\text{A.5})$$

with typically $|\tilde{M}_F|^2 \sim \epsilon_F$ at normal nuclear density [52]. This estimate shows that $|\text{Im}\Sigma_F^R|$ comes into the order of ϵ_F already at sufficiently small temperatures $T \simeq \frac{1}{3}\epsilon_F$ and still increases for higher T . This defers the application of the QPA for a wide range of temperatures.

B Renormalization of the Two-Fermion Interaction

As an example we consider a theory where non-relativistic fermions interact via two-body potentials. A priori this theory has no bosons and the two-body interactions always connect two vertices of same sign, defining iV^{--} and $iV^{++} = (iV^{--})^\dagger$, while $V^{-+} = V^{+-} = 0$. Even if resummed to an effective four point interaction \mathcal{G}_0^{--} according to eq. (63) much like Bruckner G -matrix, one has an effective interaction that connects only like sign vertices.

For the following we approximate \mathcal{G}_0 by a two-point function (as for instance in Fermi-liquid theory, where the residual interaction is supposed to be local and extracted from comparison with experimental data [22,10]), while $\mathcal{G}_0^{+-} = \mathcal{G}_0^{-+} = 0$. We also suppose that \mathcal{G}_0^{++} and \mathcal{G}_0^{--} interactions are particle-hole irreducible in the t -channel (vertical in (63), c.f. [22,10]).

Starting from \mathcal{G}_0^{--} and \mathcal{G}_0^{++} one can completely bosonize the interaction in the standard way by resumming all intermediate particle-hole loop insertions

$$\mathcal{A}_{12}^{ij} = G_{12}^{ik} G_{21}^{kj}, \quad i, j \in \{-+\} \quad (\text{B.1})$$

through the Dyson equation in two by two matrix form

$$\mathcal{G} = \mathcal{G}_0 + \mathcal{G}_0 \odot \mathcal{A} \odot \mathcal{G}. \quad (\text{B.2})$$

In space-time homogeneous cases eq. (B.2) can be solved algebraically. First one defines a residual interactions through repeated \mathcal{A}^{--} and \mathcal{A}^{++} insertions as

$$\mathcal{G}_{res}^{--} = \frac{\mathcal{G}_0^{--}}{1 - \mathcal{G}_0^{--} \mathcal{A}^{--}}, \quad \mathcal{G}_{res}^{++} = \frac{\mathcal{G}_0^{++}}{1 - \mathcal{G}_0^{++} \mathcal{A}^{++}} = -\frac{\mathcal{G}_0^{--}}{1 + \mathcal{G}_0^{--} \mathcal{A}^{++}} \quad (\text{B.3})$$

Using $\mathcal{G}_0^{-+} = \mathcal{G}_0^{+-} = 0$ straight forward algebra yields

$$\begin{aligned} \mathcal{G}^{+-} &= Z \mathcal{G}_{res}^{++} \mathcal{A}^{+-} \mathcal{G}_{res}^{--}, & \mathcal{G}^{-+} &= Z \mathcal{G}_{res}^{--} \mathcal{A}^{-+} \mathcal{G}_{res}^{++}, \\ \mathcal{G}^{++} &= Z \mathcal{G}_{res}^{++}, & \mathcal{G}^{--} &= Z \mathcal{G}_{res}^{--}, \end{aligned} \quad (\text{B.4})$$

for the components of the full interaction \mathcal{G} , where

$$Z = \left(1 - \mathcal{G}_{res}^{++} \mathcal{A}^{+-} \mathcal{G}_{res}^{--} \mathcal{A}^{-+}\right)^{-1} \quad (\text{B.5})$$

is a renormalization factor.

The explicit dependence of \mathcal{G}^{-+} and \mathcal{G}^{+-} on Z can be moved to a renormalization of the loop

$$\mathcal{G}^{-+} = \mathcal{G}_{res}^{--} \mathcal{A}_{ren}^{-+} \mathcal{G}_{res}^{++}, \quad \text{where} \quad \mathcal{A}_{ren}^{-+} = Z \mathcal{A}^{-+}. \quad (\text{B.6})$$

This full interaction \mathcal{G} has bosonic features, just describing effective bosons, such as phonons, plasmons, sigma mesons, etc. Also the inclusion of real bosons, like pions in nuclear matter, is possible, giving rise to a picture, where pions couple to pionic particle-hole excitations, see [50,10]. These effective bosons can be taken on the same footing as all other effective quanta, the fermions or other bosons, see [45,41]. Thus, effective bosons also acquire a spectral function with width and the non-diagonal components of \mathcal{G}^{-+} and \mathcal{G}^{+-} are also Wigner functions. Consequently one comes to a theory of effective in-medium fermions interacting with effective in-medium bosons.

Obviously the full (anti-)time-ordered \mathcal{G}^{--} (\mathcal{G}^{++}) depend on the in-matter densities G^{-+} and G^{+-} also via Z . However in an approximation where the value $\mathcal{G}_0^{++} \mathcal{A}^{+-} \mathcal{G}_0^{--} \mathcal{A}^{-+}$ is small, one has $Z \simeq 1$ for renormalization factor (B.5). So, one can simplify further and comes to a scheme like leading logarithmic approximation in quantum field theory, namely, a perturbation series over \mathcal{G}^{-+} (or \mathcal{G}^{+-}) neglecting corrections $1 + O(\mathcal{G}^{+-} \mathcal{A}^{-+})$ in each leading term. Such corrections are proportional to ρ^2 (or Γ^2). Thus, one approximately has

$$\mathcal{G}^{-+} = \underline{\mathbf{I}}^{\pm} \simeq \mathcal{G}_{res}^{--} \mathcal{A}^{-+} \mathcal{G}_{res}^{++} \simeq \underline{\mathbf{I}}^{\mp} \quad (\text{B.7})$$

with like-sign effective interactions (63) (whereas in the general case one comes to (B.7) with renormalized \mathcal{A}_{ren}^{-+} loops).

C Contribution of More Complicated Diagrams

Neglecting vertex corrections diagram (95) is given as

$$\begin{aligned}
 \text{---}\overset{+}{\circlearrowleft}\text{---} &= -i\Pi_{n=1}^{-+}(q) = -iV^\mu V^\nu \mathcal{A}_1^{-+}(q), \quad \text{where} \\
 -i\mathcal{A}_1^{-+}(q) &= -\int \frac{d\epsilon d^3p}{(2\pi)^4} \frac{d\omega d^3k}{(2\pi)^4} iG^{--}(p+k) iG^{++}(p-q) \\
 &\quad \times iG^{-+}(p) iG^{+-}(p+k-q) i\mathcal{G}^{-+}(k),
 \end{aligned} \tag{C.1}$$

with four-vectors $q = (\omega_q, \mathbf{q})$, $p = (\epsilon, \mathbf{k})$ and $k = (\omega, \mathbf{k})$. Here \mathcal{G}^{-+} is the "− +” interaction loop (B.7). For $q \ll k \sim p_F$ the integration in (C.1) over the \mathbf{pk} -angle gives¹⁶

$$\begin{aligned}
 J_0(\epsilon) &= \int_{-1}^1 dx G^{--}(p+k) G^{+-}(p+k-q) \\
 &= (1 - n_{\epsilon+\omega-\omega_q}) \frac{2m_F^* \pi}{pk} \frac{-\omega_q + i\Gamma \operatorname{th}((\epsilon + \omega)/(2T))}{\omega_q^2 + \Gamma^2}.
 \end{aligned} \tag{C.2}$$

Since $|x| < 1$ one has the following restrictions on p

$$\epsilon_p = p^2/2m_F^* > \epsilon_0 = (\omega - k^2/2m_F^* - \omega_q)^2 m_F^*/2k^2. \tag{C.3}$$

Further integrations can only be done in certain limits. For $\Gamma, \omega_q \ll T$ one can use Kadanoff–Baym ansatz (87), c.f. Appendix A, (A.1). In that case the ϵ integration can be performed. One needs only the real part of expression (C.1) since the imaginary part is cancelled by the corresponding diagram with opposite time ordering (opposite line sense). Thus,

$$\begin{aligned}
 J_1 &= \operatorname{Re} \int_{-\infty}^{\infty} d\epsilon G^{++}(p-q) G^{-+}(p) J_0(\epsilon) \\
 &\simeq n_{\epsilon_p - \mu_F} (1 - n_{\epsilon_p - \mu_F + \omega - \omega_q}) \frac{2m_F^* \pi^2}{pk} \frac{\omega_q^2 - \Gamma^2 u}{(\omega_q^2 + \Gamma^2)^2},
 \end{aligned} \tag{C.4}$$

where

¹⁶ using also q, k and p for $|\mathbf{q}|$, etc.

$$u = \text{th} \frac{\epsilon + \omega}{2T} \text{th} \frac{\epsilon - \omega_q}{2T} = 1 - 2n_{\epsilon - \omega_q}(1 - n_{\epsilon + \omega}) - 2n_{\epsilon + \omega}(1 - n_{\epsilon - \omega_q}) \quad (\text{C.5})$$

$$\simeq 1 - 2n_{\epsilon_p - \mu_F - \omega_q}(1 - n_{\epsilon_p - \mu_F + \omega}) - 2n_{\epsilon_p - \mu_F + \omega}(1 - n_{\epsilon_p - \mu_F - \omega_q}).$$

For low fermion occupations u is about unity and we obtain with the help of relation (78)

$$-i\mathcal{A}_1^{-+} = C_1(\omega_q) \int \frac{m_F^{*2}}{16\pi^4 \omega_q^2} n_\omega^B n_{\omega_q - \omega}^B \text{Im}\Sigma_{0,B}^R(\omega, k) J_2(\omega, k) k dk d\omega, \quad \text{with} \quad (\text{C.6})$$

$$J_2(\omega, k) = \int_{\epsilon_0}^{\infty} (n_{\epsilon_p - \mu_F + \omega - \omega_q} - n_{\epsilon_p - \mu_F}) d\epsilon_p, \quad C_1(\omega_q) = \omega_q^2 \frac{\omega_q^2 - \Gamma^2}{(\omega_q^2 + \Gamma^2)^2}.$$

The integral in eq. (C.6) can be expressed through \mathcal{A}_0^{-+} in QPA (eq. (82)), since $pk \gg m^*\Gamma$ and one obtains

$$-i\mathcal{A}_1^{-+}(\omega_q, \mathbf{q}) = C_1(\omega_q) \int \frac{\mathcal{G}^{++}(\omega, k) \mathcal{G}^{--}(\omega, k)}{4\pi^3} n_\omega^B n_{\omega_q - \omega}^B \times \text{Im}\mathcal{A}_0^R(\omega, k) \text{Im}\mathcal{A}_0^R(\omega_q - \omega, k) k^2 dk d\omega. \quad (\text{C.7})$$

This expression differs from the contribution of the corresponding QPA Feynman diagram calculated in ref. [47] only by the pre-factor $C_1(\omega_q)$ which is non-unit in our case of finite width Γ . In the QC limit this expression (C.7) coincides with the $n = 1$ term in classical Langevin result.

Diagram



$$= -i\mathcal{A}_{\text{ex}}^{-+} \quad (\text{C.8})$$

can be evaluated along similar lines considering the integrals for the left and right sub-loops

$$J_3 = \int (-1) iG^{--}(p+k) iG^{-+}(p) iG^{+-}(p+k-q) \frac{d^4 p}{(2\pi)^4} \quad (\text{C.9})$$

$$J_4 = \int (-1) iG^{++}(p_1+k-q) iG^{-+}(p_1+k) iG^{+-}(p_1) \frac{d^4 p_1}{(2\pi)^4}. \quad (\text{C.10})$$

Integration of (C.9), (C.10) is done quite analogously to the previous cases. One may integrate over $\mathbf{p}\mathbf{k}$ -angle, then over ϵ and ϵ_p in eq. (C.9) and over $\mathbf{p}_1\mathbf{k}$ -angle, ϵ_1 and ϵ_{p_1} in eq. (C.10), respectively. One recovers the corresponding QPA form derived in ref. [47], however multiplied by the pre-factor $C_0(\omega_q)$, c.f. (95).

Acknowledgments: We thank G. Bertsch, J. Bondorf, J. Cleymans, P. Danielewicz, B. Friman, K. Geiger, M. Gyulassy, P. Henning, M. Herrmann, Yu. Ivanov, J. Kapusta, I. Mishustin, B. Müller, V. Toneev and X. N. Wang for valuable suggestions

and remarks at various stages of this study. D. N. V. thanks GSI for hospitality and support. The research described in this publication was also made possible for him in part by Grant N3W000 from the International Science Foundation and the Russian Government.

References

- [1] L. D. LANDAU AND I. POMERANCHUK, *Dokl. Akad. Nauk SSSR* **92** (1953) 553, 735; also in "Collected Papers of Landau", ed. Ter Haar (Gordon & Breach, 1965) papers 75 - 77.
- [2] A. B. MIGDAL, *Phys. Rev.* **103**, (1956)1811; *Sov. Phys. JETP* **5** (1957) 527.
- [3] P. L. ANTHONY, ET AL., *Phys. Rev. Lett.* **75** (1995) 1949.
- [4] J. KNOLL AND D. N. VOSKRESENSKY, *Phys. Lett. B* **351** (1995) 43.
- [5] X.N. WANG AND M. GYULASSY, *Nucl. Phys.* **B420** (1994) 583.
- [6] "Proceedings of the Tenth International Conference on Ultra-Relativistic Nucleus-Nucleus Collisions", eds: E. Stenlund, H. -A. Gustafsson, A.Oskarsson and I.Otterlund (North-Holland, 1994); *Nucl.Phys.* **A566** (1994) 1c.
- [7] S. L. SHAPIRO AND S. A. TEUKOLSKY, "Black Holes, White Dwarfs, and Neutron Stars: The Physics of Compact Objects", Wiley and Sons (1983) chapt. 10.
- [8] "Neutron Stars", ed. by D. Pines, R. Tamagaki and S. Tsuruta, Addison-Weseley, N. Y. (1992).
- [9] G. RAFFELT AND D. SECKEL, MPI-Ph/93-90.
- [10] A. B. MIGDAL, E. E. SAPERSTEIN, M. A. TROITSKY AND D.N.VOSKRESENSKY, *Phys. Rep.* **192** (1990) 179.
- [11] N. S. TSAMIS AND R. P. WOODARD, *Ann. Phys. (N. Y.)* **238** (1995) 1.
- [12] V. SPICKA AND P. LIPAVSKY, *Phys. Rev. Lett.* **73** (1994) 3439.
P. LIPAVSKY, V. SPICKA AND B. VELICKY, *Phys. Rev.* **B34** (1986) 6933.
- [13] J. RAMMER AND H. SMITH, *Rev. Mod. Phys.* **58** (1986) 323.
- [14] M. B. GAVELA, P. HERNANDEZ, J. ORLOFF, O. PENE AND C. QUIMBAY, *Mod. Phys. Lett. A* **9** (1994) 795.
- [15] P. HUET AND E. SATHER, *Phys. Rev. D* **51** (1995) 379.
- [16] J. CLEYMANS, V.V. GOLOVIZNIN, AND K. REDLICH, *Phys. Rev.* **D47** (1993) 173 and 989.
- [17] R. KUBO, *J. Phys. Soc. Jpn.* **12** (1957) 570;
C. MARTIN AND J. SCHWINGER, *Phys. Rev* 115 (1959) 1342.
- [18] J. KNOLL AND C. GUET, *Nucl. Phys.* **A494** (1989) 334;
M. DURAND AND J. KNOLL, *Nucl. Phys.* **A496** (1989) 539.
- [19] J. KNOLL AND R. LENK, *Nucl. Phys.* **A 561** (1993) 501.
- [20] R. BAIER, YU. L. DOKSHITZER, S. REIGNE AND D. SCHIFF, Bielefeld BI-TP 94/57.
- [21] E. M. LIFSHIZ AND L. P. PITAEVSKII, "Statistical Physics", p. 2, Nauka, 1978; Pergamon press, 1980.
- [22] A. B. MIGDAL, "Theory of Finite Fermi Systems and Properties of Atomic Nuclei", Wiley and sons, 1967, Nauka, 1983.
- [23] N. P. LANDSMANN, *Phys. Rev. Lett.* **60** (1988) 1990; *Ann. Phys. (N. Y.)* **186** (1988) 141.
- [24] J. SCHWINGER, *J. Math. Phys.* **2** (1961) 407.

- [25] L. P. KADANOFF AND G. BAYM, "Quantum Statistical Mechanics", Benjamin, 1962.
- [26] L. M. KELDYSH, *ZhETF* **47** (1964) 1515; in Engl. translation *Sov. Phys. JETP* **20** (1965) 1018.
- [27] P. DANIELEWICZ, *Ann. Phys. (N. Y.)* **152** (1984) 239.
- [28] G. BERTSCH AND S. DAS GUPTA, *Phys. Rep.* **160** (1988) 189.
- [29] W. BOTERMANS AND R. MALFLIET, *Phys. Rep.* **198** (1990) 115.
- [30] M. SCHÖNHOFEN, M. CUBERO, B. FRIMAN, W. NÖRENBERG AND GY. WOLF, *Nucl. Phys.* **A572** (1994), 112.
- [31] D. N. VOSKRESENSKY, D. BLASCHKE G. RÖPKE AND H. SCHULZ, *Intern. Mod. Phys. J., E* **4** (1995) 1.
- [32] P. A. HENNING, *Nucl. Phys.* **A 582** (1995) 633.
- [33] P. A. HENNING, *Phys. Rep.* **C 253** (1995) 235.
- [34] P. DANIELEWICZ, G. BERTSCH, *Nucl. Phys.* **A533** (1991) 712.
- [35] M. HERRMANN, B. L. FRIMAN, W. NÖRENBERG, *Nucl. Phys.* **A560** (1993) 411.
- [36] P. A. HENNING AND R. SOLLACHER, preprint GSI-95-04.
- [37] E. QUACK, P. A. HENNING, *Phys. Rev. Lett.* **75** (1995) 2811; and preprint GSI-95-42.
- [38] E. M. LIFSHIZ AND L. P. PITAEVSKII, "Physical Kinetics" Nauka, 1979; Pergamon press, 1981.
- [39] H. BETHE AND E. SALPETER, "Quantum Mechanics of One and Two Electron Atoms", Springer, Berlin, 1957.
- [40] A. DESHALIT AND H. FESHBACH, "Theoretical Nuclear Physics", vol. I; "Nuclear Structure", ch. VIII. 3, Wiley, New York, 1974.
- [41] D. N. VOSKRESENSKY AND A. V. SENATOROV, *Yad. Fiz.* **45** (1987) 657; in Engl. translation *Sov. J. Nucl. Phys.* **45** (1987) 411.
- [42] R. D. PISARSKI, *Nucl. Phys.* **A525** (1991) 175c;
E. BRAATEN, *Nucl. Phys. (Proc. Suppl.)* **B23** (1991) 351.
- [43] R. BAIER, S. PEIGNE AND D. SHIFF, *Z. Phys.* **C62** (1994) 337.
- [44] P. A. HENNING, *Phys. Lett.* **B 272** (1991) 186; *Z. Phys.* **A 345** (1993) 227.
- [45] D. N. VOSKRESENSKY AND A. V. SENATOROV, *ZhETF* **90** (1986) 1505; in Engl. translation *Sov. Phys. JETP* **63** (1986) 885.
- [46] A.J. NIEMI AND W. SEMENOFF, *Nucl. Phys.* **B230** (1984) 181.
- [47] D. N. VOSKRESENSKY AND A. V. SENATOROV, *Yad. Fiz.* **52** (1990) 447; in Engl. translation *Sov. J. Nucl. Phys.* **52** (1990) 284.
- [48] C. GREINER, K. WAGNER, AND P.G. REIHARD, *Phys. Rev. C* **49** (1994) 1693.
- [49] K. MORAWETZ AND G. ROEPKE, *Phys. Rev. E* **51** (1995) 4246.
- [50] D. N. VOSKRESENSKY, *Nucl. Phys.*, **A555** (1993), 293.
- [51] M. SCHMIDT, G. ROEPKE AND H. SCHULZ, *Ann. Phys. (N. Y.)* **202** (1990) 57.
- [52] D. N. VOSKRESENSKY AND A. V. SENATOROV, *Yad. Fiz.* **53** (1991) 1521; in Engl. translation *Sov. J. Nucl. Phys.* **53** (1991) 935.
- [53] P. A. HENNING AND H. UMEZAWA, *Nucl. Phys.* **A571** (1994) 617.
- [54] B. L. FRIMAN AND O. V. MAXWELL, *Astroph. Journ.* **232** (1979) 541.
- [55] R. F. SAWYER AND A. SONI, *Astroph. Journ.* **230** (1979) 859;
R. F. SAWYER, *Astroph. Journ.* **237** (1980) 187.
- [56] P. MOREL AND P. NOZIÈRES, *Phys. Rev.* **126** (1962) 1909.
- [57] F. E. LOW, *Phys. Rev.* **110** (1958) 974.